Design Procedure for Bridge Foundations Subject to Liquefaction-Induced Lateral Spreading

WA-RD 874.2

Pedro Arduino
Christopher R. McGann
Alborz Ghofrani

April 2017

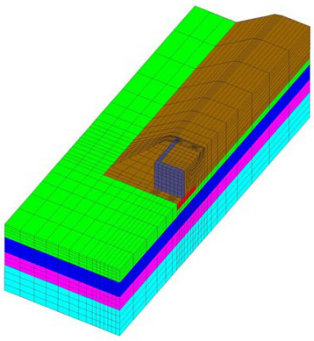

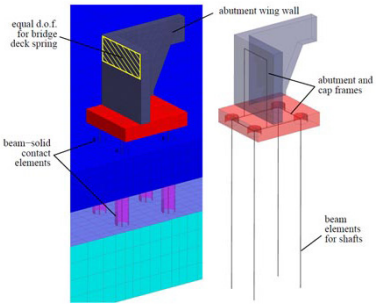

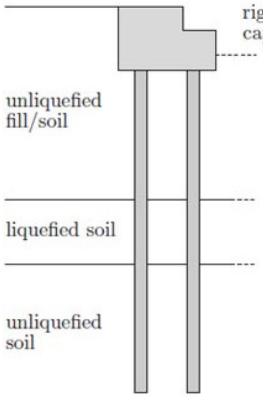

piled bridge foundation

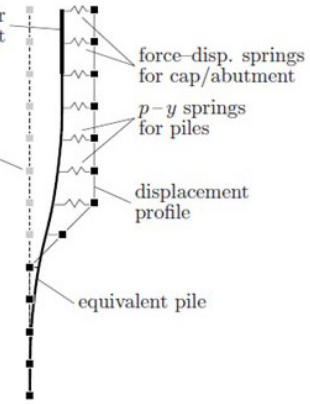

foundation model

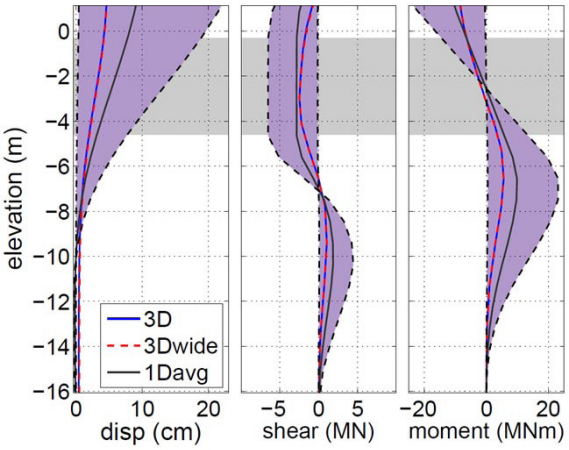

Washington State Department of Transportation
Office of Research & Library Services

WSDOT Research Report

17-10-0409

Research Report
Research Project WA-RD 874.2

Design procedure for Bridge Foundations Subject to Liquefaction-Induced Lateral Spreading

Addendum to the Final Report to
Washington State Department of Transportation (WSDOT)

by

Pedro Arduino

Christopher R. McGann

Alborz Ghofrani

University of Washington

Department of Civil and Environmental Engineering

2017

TECHNICAL REPORT DOCUMENTATION PAGE

1. Report No. WA-RD 874.2	2. Government Accession No.	3. Recipient's Catalog No.
4. Title and Subtitle Design Procedure for Bridge Foundations Subject to Liquefaction-Induced Lateral Spreading		**5. Report Date** April 2017 **6. Performing Organization Code**
7. Author(s) Pedro Arduino, Christopher McGann, Alborz Ghofrani		**8. Performing Organization Report No.**
9. Performing Organization Name and Address Washington State Transportation Center (TRAC) University of Washington, Box 354802 University District Building, 1107 NE 45th Street, Suite 535 Seattle, Washington 98105-4631		**10. Work Unit No.** **11. Contract or Grant No.** **Agreement T4118 Task 86**
12. Sponsoring Agency Name and Address Washington State Department of Transportation, Research Office Transportation Building, MS 47372 Olympia, Washington 98504-7372 Project Manager: Lu Saechao, 360-705-7260		**13. Type of Report and Period Covered** Final Research Report **14. Sponsoring Agency Code**

15. Supplementary Notes

Conducted in cooperation with the U.S. Department of Transportation, Federal Highway Administration.

16. Abstract

The response of piled bridge foundations to liquefaction-induced lateral soil deformation is an important design consideration in seismically active regions. Recent research and case history data suggest that three-dimensional deformation of the approach embankment can significantly influence the loads placed on the embedded foundations during a flow failure or lateral spreading event. For example, the 2010 Maule earthquake in Chile caused widespread lateral spreading in the soil surrounding the Mataquito River bridge, however, only insignificant structural damage was observed in the bridge itself. The discrepancy between the amount of soil deformation and structural damage suggests that design procedures for this load case that do not make adequate consideration for 3D soil deformation mechanisms may lead to overly conservative and expensive design solutions. In contrast, observed lateral spreading and damage near the Llacolén bridge was more relevant and resulted in the collapse of one of the approach sections. The Llacolén bridge approaches show lesser 3D effects on both sides of the bridge and therefore larger loads on the structural components. In this work, finite element models of the Mataquito River and Llacolén bridges are created using the OpenSees computational framework to investigate possible reduction in foundation loads during lateral spreading implied by the observed structural damage at the sites. These models include beam on nonlinear Winkler foundation models, dynamic effective stress models of the bridge-foundation-soil system in plane strain, and 3D models of the bridge abutments, approach embankments, and surrounding soils. This numerical work seeks to frame load reduction mechanisms in the context of a simplified analysis procedure for the lateral spreading load case. The results of the numerical models for the Mataquito and Llacolén bridges, along with a preliminary parameter study conducted using an independent set of 3D finite element models, indicate that consideration for the 3D geometry of the bridge site and structure may result in tangible reductions in foundation bending demands and abutment displacements compared to those returned by a plane strain description of the problem or simplified analysis using 1D models. This analysis procedure is modified to better consider the findings of this work and it is recommended to use in the design of bridge foundations subjected to lateral spreading. Finally, an approach is proposed to estimate the reductions in abutment displacement and associated foundation bending demands for a given site geometry. The latter is based on results from a preliminary parametric study and would require further development and validation to use in practice.

17. Key Words	18. Distribution Statement
Lateral spreading, Deep Foundations, Drilled Shafts, Soil Liquefaction, Lateral Loads, Liquefaction-Induced Lateral Displacements	No restrictions. This document is available through the National Technical Information Service, Springfield, VA 22161.

19. Security Classif. (of this report)	20. Security Classif. (of this page)	21. No. of Pages	
None	None		

DISCLAIMER

The contents of this report reflect the views of the authors, who are responsible for the facts and the accuracy of the data presented herein. The contents do not necessarily reflect the official views or policies of the Washington State Transportation Commission, Department of Transportation, or the Federal Highway Administration. This report does not constitute a standard, specification, or regulation.

TABLE OF CONTENTS

LIST OF FIGURES

LIST OF TABLES

Chapter 1
INTRODUCTION

Seismic design of bridge foundations is a significant aspect to the general design process for bridges in certain parts of the world. For river-spanning bridges, a critical part of the seismic design effort is an assessment of the effects of liquefaction-induced flow failure or lateral spreading on the bridge foundations. Current design procedures for this load case generally prescribe simplified analytical methods based on a two-dimensional description of the site geometry. The assumption of plane strain for for approach embankments built with finite lateral extents is a practical approach that will typically lead to conservative foundation designs.

In this report a recently proposed design approach for bridge foundations subject to liquefaction-induced lateral spreading accounting for pile pinning and 3D effects in a simplified manner is discussed. This approach is based on the research by Ashford et al. (2011) and is recently adopted by the California Department of Transportation (Caltrans) procedure. The design procedure is also based off of the applicable American Association of State Highway and Transportation Officials bridge design specifications (AASHTO, 2010a,b) and relies on an equivalent nonlinear static analysis methodology using the Beam on Nonlinear Winkler Foundation (BNWF) theory and limit equilibrium slope stability analyses.

The method was validated through comparison with two 3D finite element numerical analyses for two Chilean bridges (Mataquito and Llacolén) subject to 2010 Maule earthquake. The Mataquito bridge was selected to validate a case where the resistance of the foundation system would to some extent impede the soil movement resulting from lateral spreading. The Llacolén bridge was chosen to represent a case where the foundation system presumably does not provide resistance to the movement of soil mass. In both cases the simplified method is applicable. Chapter 2 explains the simplified procedure for design of

deep foundations subjected to kinematic loads due to liquefaction-induced lateral spreading, and Chapter 3 presents the application of the simplified method to the Mataquito and Llacolén bridges. Details of the 3D numerical analyses for these two bridges and corresponding validation study are available in Arduino et al. (2017).

Chapter 2

DESIGN PROCEDURE FOR BRIDGE FOUNDATIONS SUBJECT TO LIQUEFACTION-INDUCED LATERAL SPREADING

2.1 Recommended Design Guidelines for Lateral Spreading

The recommended design guidelines for lateral spreading are the same as those currently proposed by the California Department of Transportation and contained in an internal policy proposal (Caltrans, 2011). These guidelines are based off of the NCHRP (2002) design recommendations which effectively separate the design problem into two distinct cases: (1) an unrestrained ground displacement case, and (2) a restrained ground displacement case. The unrestrained ground displacement case assumes that the foundation is subject to a broad failure mass and will not provide significant resistance to lateral soil movement. The restrained ground displacement case assumes the failure mass has a limited width and that the foundation provides resistance to soil deformation during lateral spreading. The design processes for the restrained and unrestrained ground displacement cases, per Caltrans (2011), are described in the following discussion.

2.1.1 Restrained Ground Displacement Case

The restrained design case applies to foundations which are assumed to provide partial restraint to soil flow during lateral spreading. The prototype for this case is an approach embankment acting on a pile-supported abutment, see Figure 2.1. Due to the limited width of the embankment, it is assumed that the lateral stiffness of the abutment foundation will provide resistance to soil movement. The procedure recommended for this design case is based on the pile pinning analysis concept (Martin et al., 2002) as refined and expanded upon by later works (Zha, 2004; Boulanger et al., 2006; Ashford et al., 2011). In the pile pinning approach, a beam on nonlinear Winkler foundation (BNWF) model of the foundation is combined with a limit equilibrium slope stability analysis of the embankment to determine

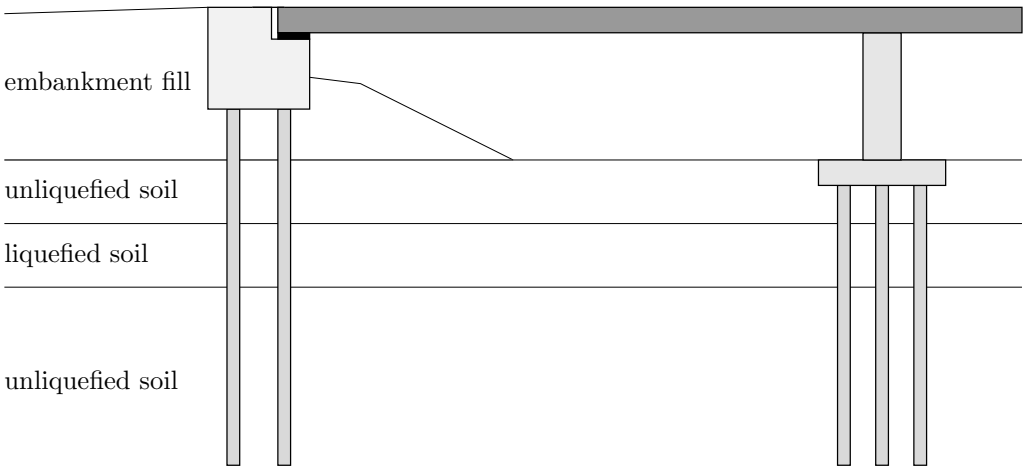

Figure 2.1: Prototype examples for restrained and unrestrained ground displacement cases.

the force-displacement state at which the resistance of the foundation is compatible with the deformation of the lateral spreading mass. The method consists of 7 basic steps:

1. **Assess Liquefaction Potential**

   The liquefaction potential of the site soils is characterized for a peak ground acceleration (PGA) corresponding to a 5% in 50 years hazard. This is typically accomplished using a simplified approach (e.g., Youd et al., 2001). Per AASHTO (2010b), the assumption of reduced strength due to pore pressure build-up or full liquefaction is required for soils with a factor of safety against liquefaction less than 1.2.

2. **Estimate Residual Strength of Liquefied Soils**

   There are two options which can be used to account for the residual strength of the *p*-*y* curves representing liquefied layers in the BNWF model of the soil-foundation system. No explicit preference of method is stated in Caltrans (2011).

   (a) The *p*-multiplier (m_p) approach (e.g., Brandenberg et al., 2007b) may be used to obtain scaled *p*-*y* curves for liquefied soils based on a sand-type backbone curve.

(b) The residual strength of the liquefied soil may be estimated using an empirically-based method (e.g., Wang, 2003), and used as the ultimate resistance in the definition of p-y curves for liquefied soils based on a clay-type backbone curve.

3. **Develop Foundation Model**

The numerical BNWF model used to analyze the foundation requires definitions for the equivalent beam representing the foundation, the p-y curves for soil-pile interaction, and a force-displacement curve to capture abutment-embankment interaction. The commercial software LPILE is typically used for this purpose.

(a) ***Definition of equivalent beam:*** The equivalent beam used to model the foundation (piles and cap/abutment) may be defined assuming linear elastic or nonlinear elastoplastic behavior. In both cases, the spatial arrangement of the piles is largely ignored and the equivalent beam is developed in a simplified manner. For linear elastic behavior, the equivalent beam model is obtained by multiplying the bending stiffness, EI, of a single pile by the number of piles in the group. For nonlinear behavior, the moment-curvature response of a single pile is scaled by the number of piles in the group.

The pile cap/abutment is incorporated into the equivalent beam using a large linear elastic bending stiffness which approximates its rigidity relative to the piles. The rotational stiffness of the pile group is modeled using a rotational restraint located at the connection of the piles to the cap/abutment. This restraint is assigned a stiffness equivalent to the estimated rotational stiffness of the pile group after Mokwa and Duncan (2003).

(b) ***Definition of p-y curves for piles:*** The p-y curves used for soil-pile interaction are based on the work of Matlock (1970) for soft clay, Reese and Welch (1975) for stiff clay, and Reese et al. (1974) for sand. The base p-y curves determined for the site using these methods are modified to account for pile group effects and the effects of liquefaction.

- Group effects are considered using a composite group efficiency factor computed as the average of the reduction factors for each row in the pile group as recommended by Mokwa and Duncan (2001).
- The *p-y* curves of liquefied soils are defined as discussed in step 2. The influence of the weaker layer of liquefied soil on the surrounding material is accounted for using a linearly smeared ultimate lateral resistance profile as shown in Figure 2.2.

(c) ***Definition of cap/abutment-soil interaction curve:*** A tri-linear force-displacement curve describing the interaction of the cap/abutment with the surrounding soil is defined using the maximum passive load of the soil on the foundation, F_{ult}, and the displacement, Δ_{max}, required to mobilize this force. This curve is shown in Figure 2.3. Two failure cases are considered to determine F_{ult}, with the lesser force controlling the design. The two cases are as follows:

- A log-spiral passive wedge acting on the cap/abutment combined with the lateral resistance provided by the portions of the piles extending through the crust (i.e., soil above the liquefied layer).
- A Rankine passive wedge acting on foundation elements above the liquefied layer assuming that the cap/abutment, crust soil beneath the cap/abutment, and piles within the crust all act as a composite block.

The displacement, Δ_{max}, corresponding to the ultimate passive force is taken as the sum of 5% of the cap/abutment height with an adjustment factor which accounts for the effects of the depth of the liquefied material and the transverse thickness of the cap/abutment after Brandenberg et al. (2007a).

4. **Displacement Analysis of Foundation Model**

Once the foundation model has been completed, a series of pushover analyses are conducted in which increasing crustal displacements are considered. Displacements are applied to the soil end of the *p-y* springs using the displacement profile shown in Figure 2.4 to simulate the effects of lateral spreading. For a series of increasing surface

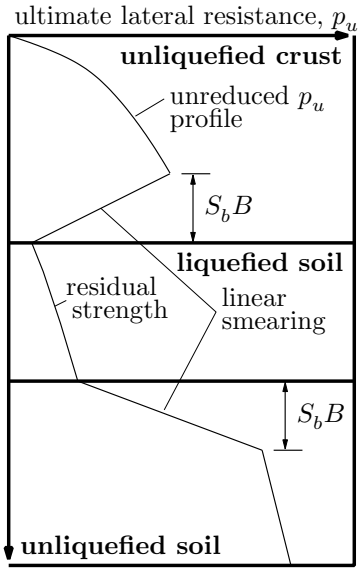

$$S_b = \begin{cases} 2, & B < 1 \text{ ft} \\ 2 - (B-1)/2, & 1 \text{ ft} \leq B \leq 3 \text{ ft} \\ 1, & B > 3 \text{ ft} \end{cases}$$

where B is the pile diameter (units of ft)

Figure 2.2: Smeared profile of ultimate lateral resistance to account for presence of liquefied layer on strength of surrounding soil (after Caltrans, 2011).

displacements, the pile cap displacement and a running average of the shear force at the center of the liquefied layer are recorded to obtain a lateral spreading pushover curve for the foundation.

The running average shear force for each displacement increment is computed as the sum of the current and all previous shear force values divided by the number of terms in the sum. This running average is made in an attempt to account for the discrepancy between the pushover analysis of this design step, in which the shear force increases with increasing ground displacement, and the slope deformation analyses of the next step, in which only constant foundation resisting forces are considered.

5. **Slope Stability and Deformation Analysis of Approach Embankment**

A pseudo-static slope stability model is used to determine foundation resisting forces, R, at the center of the liquefied layer for a series of horizontal accelerations, k_h, applied in the model as a constant inertial force

$$F_h = k_h W \tag{2.1}$$

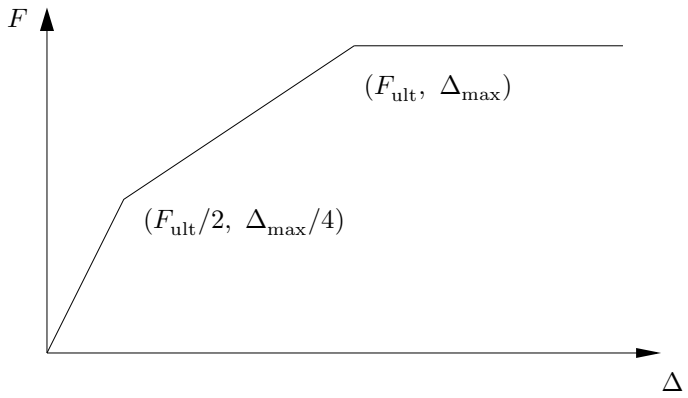

Figure 2.3: Tri-linear force-displacement curve for pile cap/abutment-soil interaction in foundation model (after Caltrans, 2011).

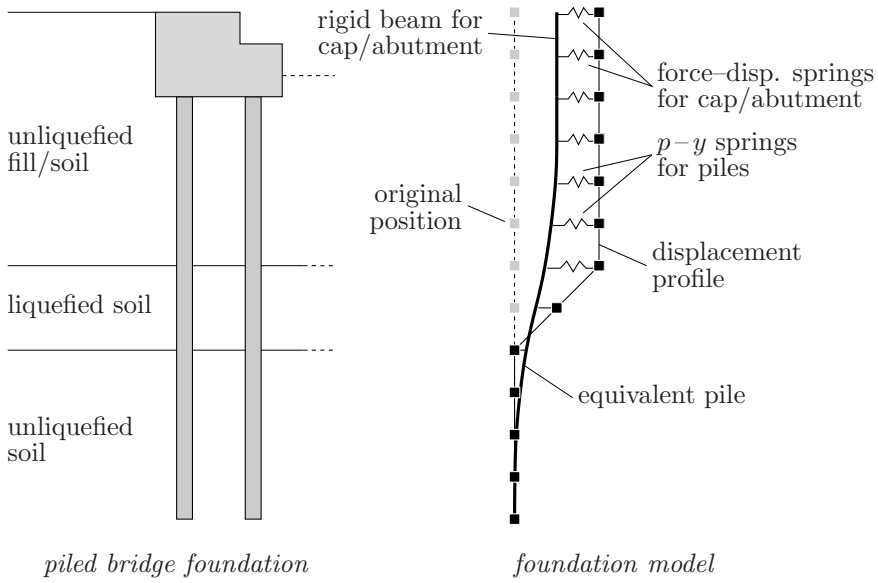

Figure 2.4: Transition from physical bridge foundation to foundation model showing the applied displacement profile for lateral spreading pushover analysis.

where W is the weight of the failure mass. For each considered acceleration value, the resisting force for which the slope factor of safety reaches 1.0 is recorded.

In these analyses, the restraining forces are applied on the lower edge of the failure surface, and the failure surface is constrained to the center of the liquefied layer, as

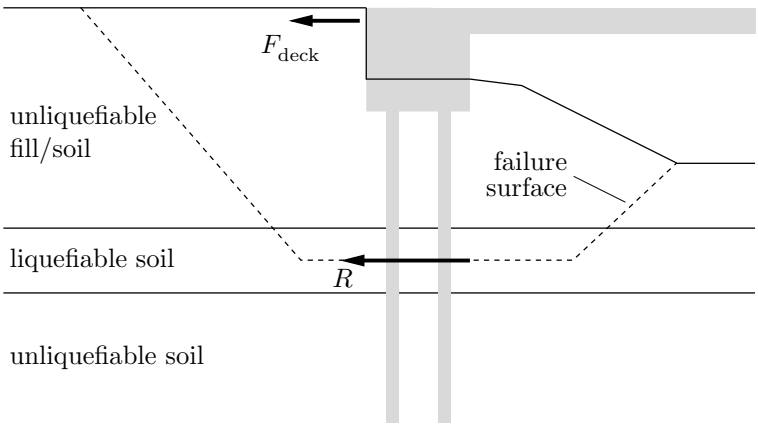

Figure 2.5: Schematic of slope stability analysis considering a deck resisting force, F_{deck}, and foundation resisting force, R.

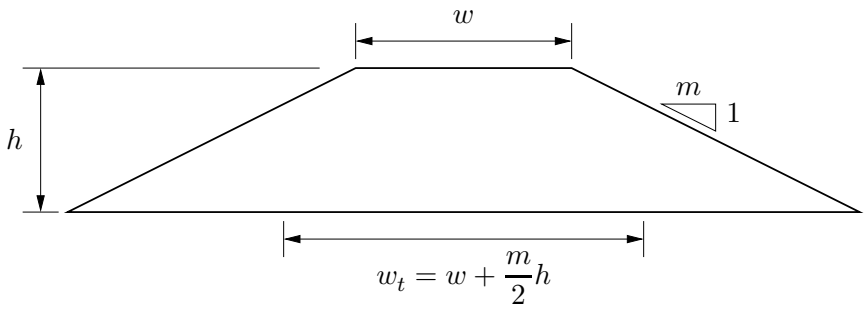

Figure 2.6: Tributary width of embankment, w_t (after Boulanger et al., 2006).

depicted in Figure 2.5. It is also recommended that the failure surface be limited to extending ≤ 4 times the height of the embankment away from the bridge abutment. If it is assumed that the bridge deck will provide longitudinal resistance to abutment movement, a deck resisting force, F_{deck}, is computed based on the full passive resistance of the soil acting on the deck and applied during the slope stability analysis.

Newmark rigid sliding block analysis is used to compute the slope displacements corresponding to the k_h coefficients used to determine resisting forces in the slope stability analyses. Typically, a simplified procedure (e.g., Bray and Travasarou, 2007) is used in lieu of site-specific sliding block analysis.

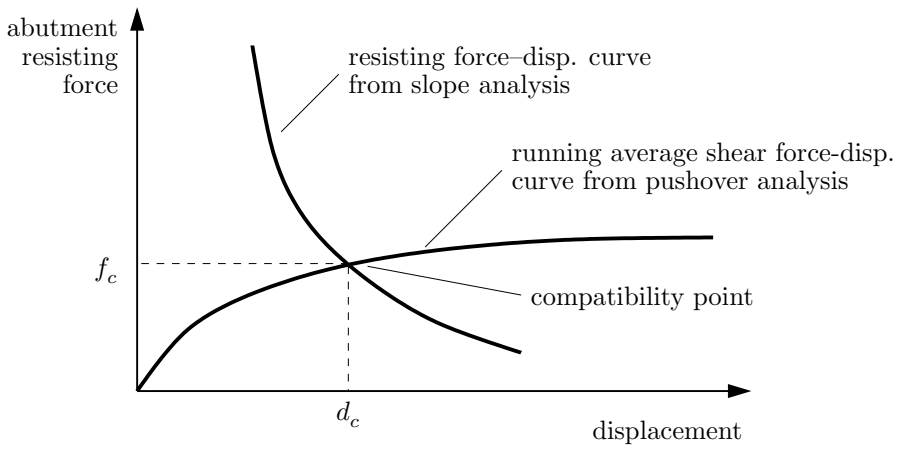

Figure 2.7: Determination of compatible force-displacement state.

6. **Determine Force-Displacement Compatibility**

The results of the pushover and slope stability/deformation analyses are used to determine a compatible force-displacement state which considers the restraining effects of the bridge foundation on the deformation of the soil-foundation system during lateral spreading. This is accomplished by plotting the slope force-displacement curve determined from the slope stability/deformation analyses (step 5) with the foundation running average shear force-displacement curve determined in the pushover analyses (step 4) in the manner shown in Figure 2.7.

The running average forces are used for the foundation force-displacement curve to account for the differences in how the resisting force is handled in the two curves (constant in the slope deformation curve, non-constant in the pushover curve). Because the resisting forces obtained in the slope stability phase represent a force per unit thickness of soil, the lateral spreading pushover curve must be scaled by an appropriate width. For this purpose, the finite transverse thickness of an approach embankment is considered in the scaling factor, as the pushover curve forces are divided by the tributary width of the embankment determined as shown in Figure 2.6.

7. **Assess Foundation Performance**

The final performance evaluation for the foundation is conducted using a lateral spreading pushover analysis which considers the combined effects of kinematic and inertial loads. A kinematic loading is applied using the displacement profile shown in Figure 2.4 with an applied surface displacement set as the compatible displacement, d_c, determined in step 6. Consideration for inertial effects is made during this analysis by applying 50% of the inertial loads from any associated superstructure or pile caps, as it is unlikely that lateral spreading occurs during peak shaking.

The inertial effects of superstructure elements for typical bridge bents are considered using an applied moment and shear force pair, which are determined based on the design of the bridge columns. There are two possibilities:

(a) In most cases, the bridge columns are designed to yield and develop plastic hinges prior to the onset of yield in the foundation elements. For this type of design, the inertial moment is set at 1.2 times the plastic moment capacity of the column. For columns which have a pinned connection at the top and a fixed connection at the bottom (free-fixed configuration), the inertial shear force is determined by dividing this inertial moment by the height of the bridge column. For columns with a fixed-fixed configuration, the inertial shear force is set as the inertial moment divided by one-half the column height.

(b) If the column is not expected to yield for the design event, then the inertial shear force is estimated as the product of the tributary mass carried by the bridge column with the spectral acceleration corresponding to the first mode of the column. The inertial moment is set as the product of the inertial shear force with the column height for a free-fixed configuration, or one-half of the same product for a fixed-fixed configuration.

For seat-type abutment foundations, the superstructure is supported by bearings which can freely rotate, and the only means of transferring inertial shear from the superstructure is through a backwall, typically designed as a weak fuse with limited capacity to transfer load. For these reasons, it is assumed that no inertial loads

are transferred from the superstructure for seat-type abutments. To account for the inertial effects of relatively massive foundation bodies, such as a pile cap, an inertial force is computed as

$$f_{\text{cap}} = 0.65 m_{\text{cap}} a_{\text{no liq}} \tag{2.2}$$

where $a_{\text{no liq}}$ is the design PGA without consideration for liquefaction, m_{cap} is the pile cap mass, and the 0.65 factor is used to represent a reduction in PGA due to the onset of liquefaction.

The combined kinematic-inertial pushover analysis is used to determine if the foundation has sufficient capacity under an assumed peak demand case. This analysis is used to evaluate the resulting shear force and bending moment demands for the deep foundations and to assess whether the displacement at the pile cap/abutment is acceptable for the overall bridge structure.

2.1.2 Unrestrained Ground Displacement Case

The unrestrained design case applies to foundations that are assumed to be unable to significantly restrain the flow of soil associated with lateral spreading. An example case is an interior bridge bent foundation embedded in a site with broad transverse continuity as shown in Figure 2.1. In this case, the lateral stiffness of the foundation is insignificant relative to the loads applied by the lateral soil flow. For design purposes, it is assumed that soil movement will be unaffected by the presence of the foundation, though evidence from previous earthquakes shows that this is not true at the local level.

The design process for the unrestrained ground displacement case begins in the same manner as the restrained ground displacement case, with the assessment of liquefaction potential (step 1), estimation of residual strength for liquefied soils (step 2), and the definition of a foundation model (step 3) corresponding exactly. After the completion of these steps, the remaining steps for the unrestrained case differ from those previously discussed.

Estimation of the design ground displacement for the unrestrained case is initiated by evaluating the slope stability factor of safety (FS) assuming the absence of the foundation. If FS ≤ 1.05, a flow-type failure is assumed. Typically, an assumption of 5 ft of displacement

is made, as this is considered sufficient to mobilize the full passive force of the crust on the foundation, and it is stated in Caltrans (2011) that as long as the passive force is mobilized, the remaining analysis is insensitive to the specific displacement value. For cases where FS > 1.05, the crustal displacement is estimated using one of two simplified techniques. When the slope has a predictable failure surface, a Newmark sliding block-based approach (e.g., Bray and Travasarou, 2007) is used with an input acceleration set equal to the design PGA. For gentle slopes, where there is greater uncertainty in the failure surface, crustal displacements are estimated using the strain potential procedure of Faris et al. (2006).

The foundation is evaluated using a lateral spreading pushover analysis, with an applied displacement profile as shown in Figure 2.4. The imposed surface displacement in this analysis is set equal to that required to mobilize the full passive soil resistance for the FS ≤ 1.05 case, or to the estimated crustal displacement for the FS > 1.05 case. Inertial loads from the bridge superstructure (if any) are included in this analysis in the manner described in step 7 for the restrained ground deformation case. The bending moment, shear force, and displacement demands computed using the pushover analysis are compared to the allowable foundation performance criteria.

Chapter 3

EXAMPLES

3.1 Restrained Case: Puente Mataquito

The Mataquito River Bridge, constructed in 2006, spans the Mataquito River between Quivolgo and Iloca, Chile. Liquefaction-induced lateral spreading occurred on both banks of the river due to the M_w8.8 February 27, 2010 offshore Maule earthquake. The bridge has seat-type abutments founded on 4×2 drilled shaft groups, and the interior piers are supported by 3×1 groups of shafts. Lateral soil displacements of up to 2.5 m occurred near the northeast abutment, involving the approach embankment and a 100 m floodplain sloping gently toward the river. Similar lateral spreading effects were observed on the opposite bank, however, the corresponding embankment soils were not involved (FHWA, 2011).

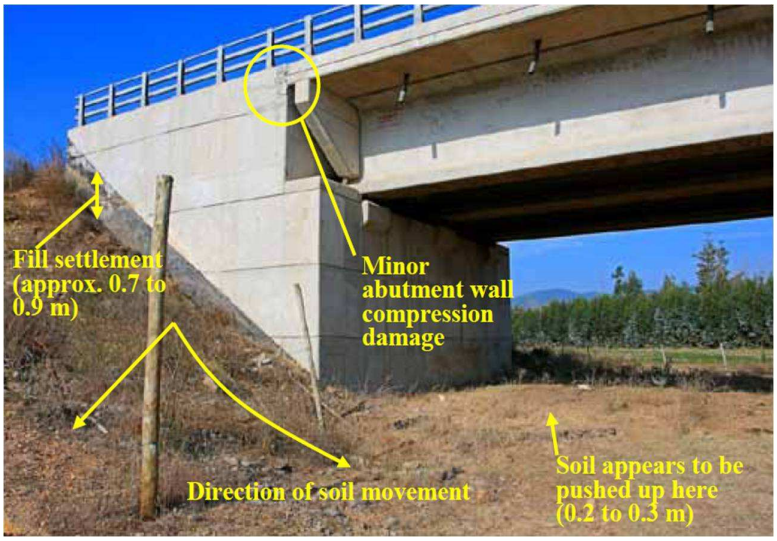

Figure 3.1: Settlement and lateral spreading deformation of northeast approach embankment to Mataquito River Bridge (FHWA, 2011).

The bridge foundations reportedly did not experience significant permanent lateral deformations, and all bridge spans remained intact and functional. The northeast approach embankment settled approximately 0.7 to 1 m relative to the bridge deck, Figure 3.1. Lon-

gitudinal roadway cracks suggest that there was a component of embankment deformation perpendicular to the bridge axis of approximately 0.6 m (GEER, 2010), indicating that some of the soil moved around the abutment rather than directly into it. This 3D effect may have reduced the forces applied to the foundations, contributing to the minimal damage and deformation observed in the bridge.

In this application example the pile pinning model of the southwest bridge abutment is created following the Caltrans (2011) procedure for the restrained ground displacement case presented in Section 2.1.1. This model is considered in order to assess the viability of this design approach through comparison with the observations made at the bridge site and the bending demands resulting from 3D finite element models (Arduino et al., 2017). To this purpose, a BNWF model of the foundation is developed by converting the 4×2 pile group (Figure 3.5) into an equivalent single shaft model, and through the definition of soil-shaft interaction (p-y) curves that appropriately represent the idealized soil profile and account for group effects. In addition to this BNWF model of the foundation, a limit equilibrium slope stability model is developed for use in determining the compatible force-displacement state which defines the final design displacement in the pile pinning approach.

3.1.1 Development of Idealized Soil Profile

The soil profile used for numerical models of the Puente Mataquito site is based on the subsurface explorations (sondajes) made at the site and the soil characterization profile reported by (Petrus, 2006). The geotechnical report for the project (Petrus, 2006) roughly divides the site into three layers, an upper loose sand layer, a middle layer of denser sand, and an underlying dense gravel layer. The spatial layout of the assumed soil profile is shown in Figure 3.2 with relevant model properties summarized in Table 3.1. Representative friction angles, ϕ, for each layer are estimated from these average SPT values using a combination of the correlations proposed by Meyerhof (1956) and Peck et al. (1974). Small strain shear and bulk moduli, $G_{\max}$ and $K_{\max}$, are estimated by correlating the assumed friction angle values to relative densities using the relation proposed in FHWA (1978). Void ratios, e, and phase transformation angles, ϕ_{pt}, are assumed based on the estimated relative densities.

Table 3.1: Model properties for soil layers in idealized soil profile.

Soil Type	ρ (Mg/m^3)	ρ_{sat} (Mg/m^3)	ϕ (°)	G_{max} (MPa)	K_{max} (MPa)	e	ϕ_{pt} (°)
loose sand	1.7	2.16	31	60	175	0.85	29
dense sand	1.7	2.11	36	90	230	0.77	27
gravel	1.7	2.08	42	130	250	0.55	32
fill	1.8	–	42	130	250	0.55	32

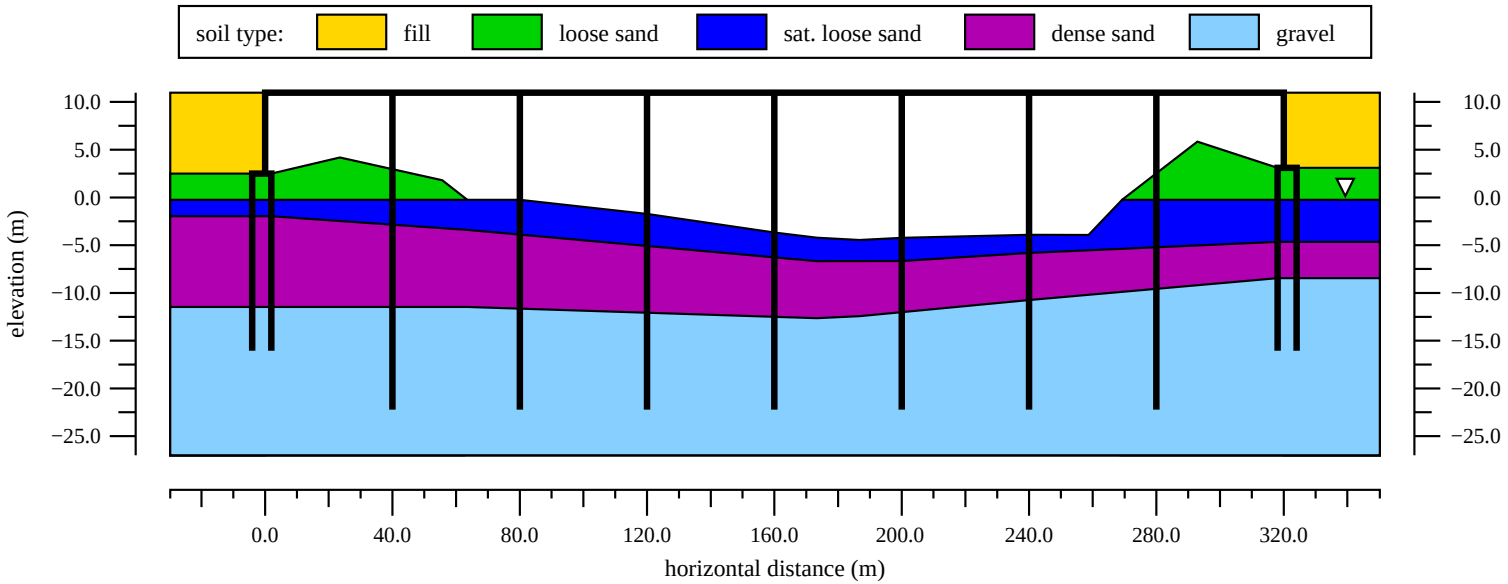

Figure 3.2: Elevation view of bridge and idealized soil profile (vertical scale increased). Horizontal datum is at the northeast bridge abutment.

3.1.2 Assessment of Liquefaction Potential

The liquefaction susceptibility of the soil at the Puente Mataquito site is assessed using the sand liquefaction triggering relationship of Youd et al. (2001). Assuming a peak ground acceleration (PGA) of 0.4 g based on the recorded PGA in downtown Concepción (Boroschek et al., 2010), a fines content in the range of 5% to 15%, an average reduction coefficient of 0.9, a magnitude scaling factor of 0.75, and a total-to-effective vertical stress ratio of 2, Ledezma (2012) estimated that sands with a normalized SPT value below 28 blows/ft are likely to liquefy in an event similar to the Maule earthquake.

For the SPT blowcount and idealized soil profiles shown in 3.2, this blow count limit indicates that the loose sand layer is highly susceptible to liquefaction and the boundaries of this layer represent the likely scope of liquefaction at the site. The underlying dense sand and gravel layers are much less likely to liquefy for the considered event. Unless otherwise noted, it is assumed in all analyses that liquefaction is confined to the saturated portion of the loose sand layer.

3.1.3 Foundation Modeling Approach

The abutments and pier foundations for Puente Mataquito are 1.5 m diameter reinforced concrete shafts. For modeling purposes, an idealized template cross-section, Figure 3.3, is assumed based on the typical reinforcement configuration used in the shaft foundations. There are 31 longitudinal bars, all 36 mm in diameter, and the central core of the shaft is confined with 18 mm diameter spiral ties spaced 10 cm apart.

A moment-curvature analysis is conducted to verify proper implementation of the fiber section model and establish the capacity of the model shaft foundation. Figure 3.4 shows the moment-curvature response of a single model shaft foundation. The maximum bending moment of 9000 kN·m compares favorably with the nominal design moment capacity for the shaft foundations used in the construction of Puente Mataquito. In some of the models used in this research, the shafts are modeled using linear elastic section behavior. This linear elastic response is defined using the initial tangent to the nonlinear moment-curvature response presented in Figure 3.4.

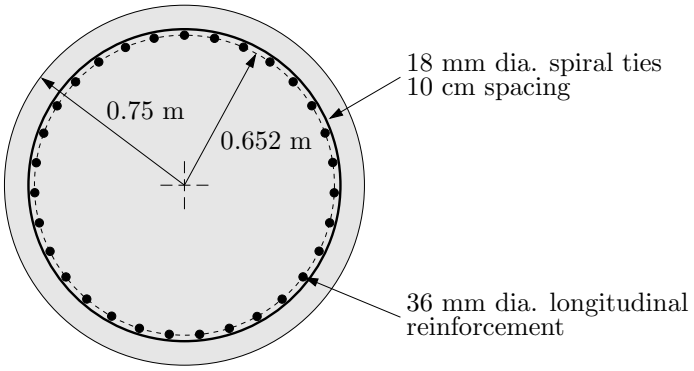

Figure 3.3: Dimensions and details of the model drilled shaft cross-section.

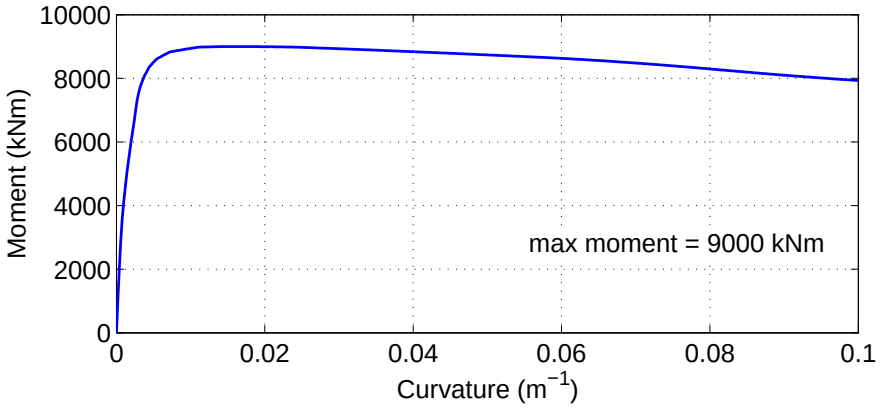

Figure 3.4: Model moment-curvature response for single drilled shaft foundation at design axial force.

At the abutments, the shafts are grouped in a 4×2 layout with the dimensions and orientation shown in Figure 3.5. The short dimension of the pile cap corresponds to the longitudinal axis of the bridge. The shafts at the abutments are 17 m long, and extend from the pile cap down into the gravel soil layer, ending at a vertical elevation of -16.06 m (see Figure 3.2). The shafts are grouped in a 3×1 configuration at the seven interior piers with the layout and dimensions shown in Figure 3.6. The interior pier shafts are 28.6 m long and extend from a concrete cap just below the bridge girders into the gravel layer, ending at an elevation of -22.22 m.

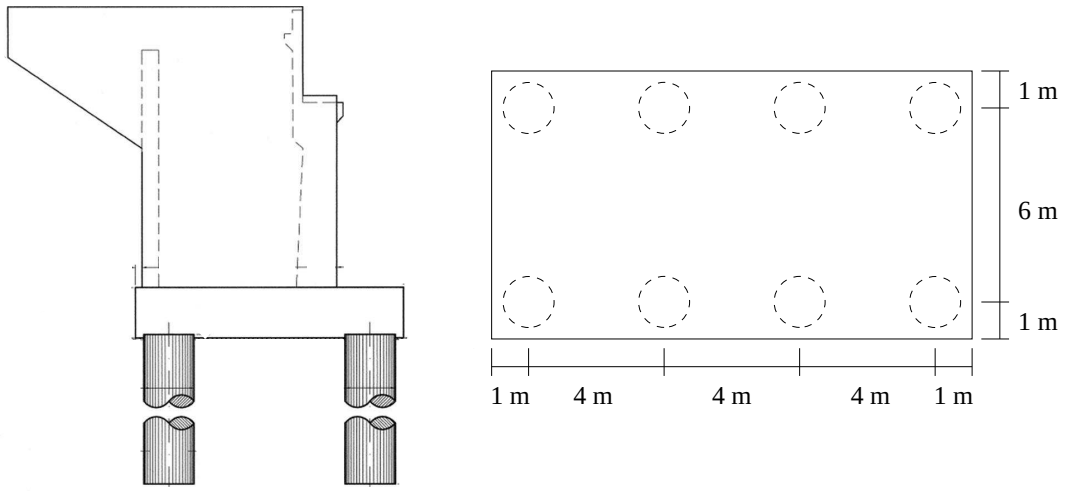

Figure 3.5: Elevation and plan views of typical abutment for Puente Mataquito (courtesy Ministerio de Obras Públicas, Chile).

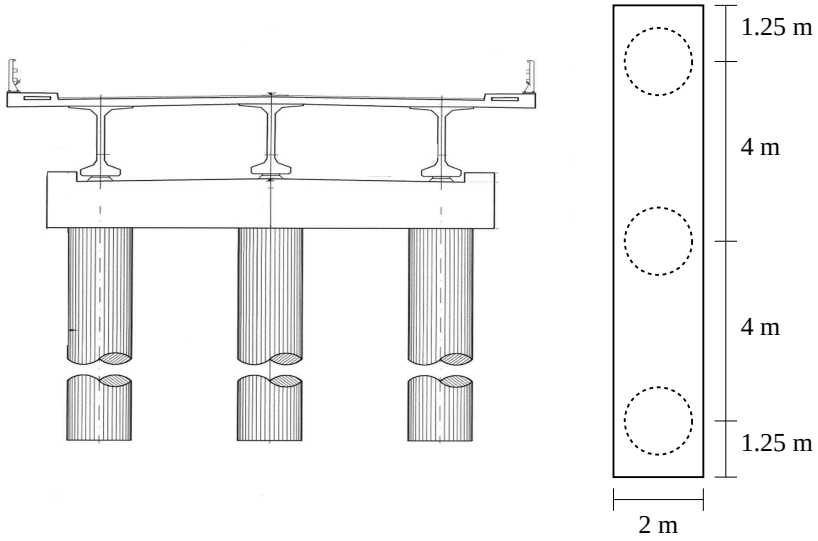

Figure 3.6: Elevation and plan views of typical interior pier shaft cap for Puente Mataquito (courtesy Ministerio de Obras Públicas, Chile).

Table 3.2: Properties of linear elastic equivalent beam model for grouped shaft foundation.

Parameter	Single Shaft	Equivalent Shaft
E	21.3 GPa	21.3 GPa
I	0.2485 m^4	1.988 m^4
A	1.7671 m^2	14.137 m^2
G	8.52 GPa	8.52 GPa

3.1.4 Development of Foundation Model

The southwest abutment foundation is converted into an equivalent beam model using the Caltrans recommendations for the pile pinning analysis procedure. Two versions of the equivalent beam model are created, one which considers a linear elastic shaft response, and one which considers the nonlinear section response of the shaft foundations. The properties of the equivalent linear elastic shaft section are determined using the geometry of the shaft and the initial bending stiffness indicated in the moment-curvature plot of Figure 3.4, which, for a single shaft, is $EI = 5.295$ GN·m^2. A gross second moment of the area for a single shaft, $I_g = 0.2485$ m^4, suggests an elastic stiffness $E = 21.3$ GPa, and, for an assumed Poisson's ratio $\nu = 0.25$, a shear stiffness $G = 8.52$ GPa. The section parameters for a single shaft are scaled by the number of shafts in the group to obtain values for use in the equivalent beam model. The properties of this linear elastic equivalent beam model are provided in Table 3.2. The nonlinear equivalent beam model is defined by scaling the single shaft moment-curvature response by the number of shafts in the group, resulting in the equivalent beam model moment-curvature response shown in Figure 3.7. The stiffness of the shaft group is likely underrepresented by the scaling approach adopted for use by Caltrans, however, the intention of this study is an evaluation of the approach, thus, the modeling recommendations involved in its use are followed here.

A rotational spring is used to simulate the rotational stiffness of the shaft cap following the procedure of Mokwa and Duncan (2003). For an axial load of $P = 4120$ kN, and assuming that the axial capacity is achieved with 0.25 in of vertical displacement, the axial

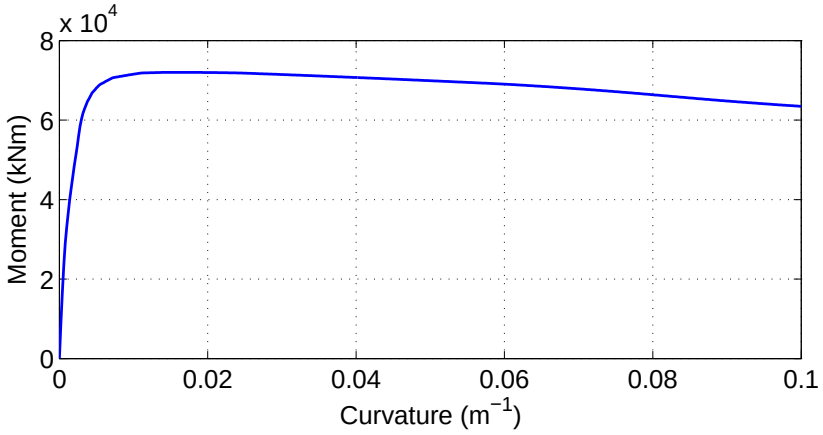

Figure 3.7: Model moment-curvature response for nonlinear equivalent beam model of grouped shaft foundation.

stiffness for a single pile is computed as

$$k_a = \frac{0.75 \cdot 4120 \text{ kN}}{0.0063 \text{ m}} = 490 \text{ MN/m} \tag{3.1}$$

The rotational stiffness for the pile group is based on the number of rows in the shaft cap, n_{row}, the number of shafts in each row, n_{pile}, and the distance from the center of the row to the center of the shaft cap, d_c, as

$$k_\theta = n_{\text{row}} n_{\text{pile}} d_c^2 \, k_a \tag{3.2}$$

For the geometry of the abutment group at Puente Mataquito,

$$k_\theta = 2 \cdot 4 \cdot (3 \text{ m})^2 \cdot 490 \text{ MN/m} = 35.3 \text{ GN} \cdot \text{m} \tag{3.3}$$

This rotational spring is applied to the equivalent beam model at the location of the shaft cap. Above this point, the beam model is given a bending stiffness that is many times larger than the rest of the beam in order to incorporate the abutment into the equivalent beam model. This relatively rigid abutment portion of the beam is assigned linear elastic behavior for both the linear elastic and nonlinear equivalent beam models.

It should be noted that the equivalent beam models defined using the Caltrans (2011)

procedure under-represent the bending stiffness of the pile group, which should fall somewhere between the values reported above and the assumption that the group acts as a single beam during the application of lateral loads. The addition of the rotational spring to the model provides some compensation, but even with this spring, the equivalent model may represent an oversimplification of the true foundation response.

3.1.5 Definition of p-y Curves

In the BNWF model, the soil response is represented by a series of *p-y* curves defined based on the idealized soil profile with the properties presented in Table 3.1. These curves are defined with ultimate lateral resistance, p_u, values computed using the method of Brinch Hansen (1961) and initial stiffness, k_T, values computed using the API (2007) recommendations corrected for overburden stress after Boulanger et al. (2003).

Group effects are incorporated into the BNWF model using the group efficiency factors of Mokwa and Duncan (2001) and the procedure recommended by Caltrans (2011). The efficiency factors for the leading and trailing rows are 0.88 and 0.67, respectively. The group effect *p*-multiplier for the equivalent shaft model is computed as the product of the number of piles with the average of the leading and trailing row values

$$p_{\text{group}} = \frac{8 \cdot (0.88 + 0.67)}{2} = 5.88 \tag{3.4}$$

The residual strength of the liquefiable soil is computed using the undrained shear strength expression recommended by Ledezma and Bray (2010)

$$\frac{S_{ur}}{\sigma'_v} = \exp\left(\frac{N_{1,60\ \text{cs}}}{8} - 3.5\right)\left(1 + \frac{\left(0.3N_{1,60\ \text{cs}}\right)^2}{128}\right) \qquad 0 \le N_{1,60\ \text{cs}} \le 20 \tag{3.5}$$

where S_{ur} is the undrained shear strength, σ'_v is the vertical effective stress, and $N_{1,60\ \text{cs}}$ is the clean sand corrected SPT blowcount. This expression is a weighted average of the procedures proposed by Seed and Harder (1990), Olson and Stark (2002), Kramer and Mayfield (2007), and Idriss and Boulanger (2007). In their approach, Ledezma and Bray assigned a weight of 3 to methods that give S_u/σ'_v (i.e. Olson and Stark (2002) and Kramer

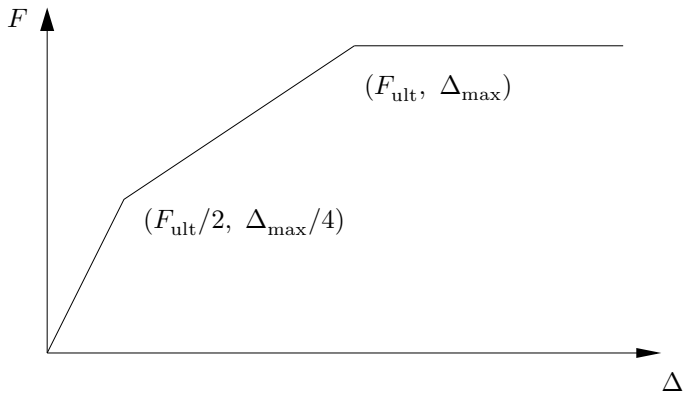

Figure 3.8: Tri-linear force-displacement curve for pile cap/abutment-soil interaction in foundation model (after Caltrans, 2011).

and Mayfield (2007)) compared to a weight of 2 assigned to methods that only give S_u. A weight of 5 was assigned to the most recent method of Idriss and Boulanger (2008). The undrained shear strength is used to define the p_u values of the *p-y* curves within the liquefiable loose sand layer, and is computed using the average SPT value assumed for this layer when defining the idealized soil profile of the site. Using this approach, the average undrained strength for the layer is 11.7 kPa, and the undrained strength varies with overburden pressure as $S_u/\sigma'_v = 0.11$. A linear smearing is used to reduce the p_u values for the *p-y* curves within one shaft diameter of the liquefiable layer boundaries per the recommendations of Caltrans (2011) and Ashford et al. (2011).

3.1.6 Definition of Abutment-Soil Interaction Curve

A tri-linear force-displacement curve is used to model abutment-embankment interaction in the BNWF model. As shown in Figure 3.8, this tri-linear curve is defined in terms of two variables, the ultimate passive force and the displacement at which this force is assumed to be fully developed. Using the geometry and properties of the embankment fill assumed for the idealized soil profile of the site, an ultimate lateral force $F_{ult} = 94$ MN is computed assuming the development of a Rankine passive wedge at a displacement of $\Delta_{max} = 0.51$ m.

3.1.7 Pseudostatic Slope Stability Model

The determination of the compatible force-displacement design state for the restrained ground displacement case requires the comparison of the results obtained from a pushover analysis of the BNWF model described in the preceding sections with the results of a slope stability analysis of the abutment site. For this purpose, a pseudostatic slope stability model is developed using Slide 6.0 (Rocscience, 2010) for the geometry and properties assumed in the idealized soil profile. This model is used to compute the horizontal resisting force required at the center of the liquefiable layer to reach a factor of safety FS = 1.0 for a series of horizontal yield accelerations $k_y = 0.05$, 0.1, 0.15, 0.2, 0.25, 0.3, 0.35, 0.4.

To assess the sensitivity of the final design result to choices made during the analysis steps, several versions of this model are developed and analyzed. Two limit equilibrium methods are considered, the simplified Bishop method (Bishop, 1955) and the simplified Janbu method (Janbu, 1973). The failure surfaces are restricted such that they do not extend more than four times the embankment thickness behind the abutment to eliminate complex effects related to a very large slide mass per the suggestion of Ashford et al. (2011). Four cases are considered for each limit equilibrium approach:

- $F_{\text{deck}} = 0$ kN/m with constant $S_u = 11.7$ kPa in the liquefiable layer.
- $F_{\text{deck}} = 377$ kN/m with constant $S_u = 11.7$ kPa in the liquefiable layer.
- $F_{\text{deck}} = 0$ kN/m with $S_u/\sigma'_v = 0.11$ in the liquefiable layer.
- $F_{\text{deck}} = 377$ kN/m with $S_u/\sigma'_v = 0.11$ in the liquefiable layer.

The non-zero F_{deck} value is determined from the full passive resistance of the embankment fill acting over the 2.74 m depth of the bridge deck, and is applied at the centroid of the bridge deck/girder cross-section. The constant undrained strength values are the average value for the layer, and the overburden dependent values correspond to the SPT profiles assumed for the idealized soil profile.

3.1.8 Application of Pile Pinning Analysis Procedure to Southwest Abutment

The BNWF equivalent shaft foundation and limit equilibrium slope stability models developed for the southwestern abutment of Puente Mataquito are used to determine compatible force-displacement states for the bridge abutment and approach embankment. The viability of this design approach is assessed through comparison with observations made at the site. The variability in the estimated compatible state is demonstrated by considering various modeling decisions and assumptions throughout the procedure, and an approach for estimating an appropriate compatible state amidst the observed variability is proposed.

3.1.9 Initial Pushover Analysis of Foundation Model

The equivalent shaft BNWF model of the southwestern abutment is analyzed in a pushover analysis simulating the kinematic demands of lateral spreading. As discussed in Section 2.1.1, this pushover analysis is conducted by applying a set displacement profile to the soil end of the *p-y* springs supporting the foundation. The applied displacement profile used for this purpose is set at a constant 1.0 m in the upper layers, linearly-increasing from zero to 1.0 m across the liquefiable layer, and zero in the underlying material as shown in Figure 3.9.

The purpose of this analysis is to obtain a curve defining the relationship between the applied surface displacement and the foundation shear force at the center of the liquefiable loose sand layer. The unmodified shear force, V_{unmod}, recorded at this location for each step in the analysis is used to compute a corresponding running average shear force, V_{run}, which, at recorded step j, is computed as

$$V_{\text{run}}(j) = \frac{\sum_{i=1}^{j} V_{\text{unmod}}(j)}{j} \tag{3.6}$$

This running average shear force, introduced by Boulanger et al. (2006), is recommended for use in subsequent analysis steps to account for a discrepancy in how the force in the middle of the liquefied layer is treated in the pushover and slope stability phases of the procedure.

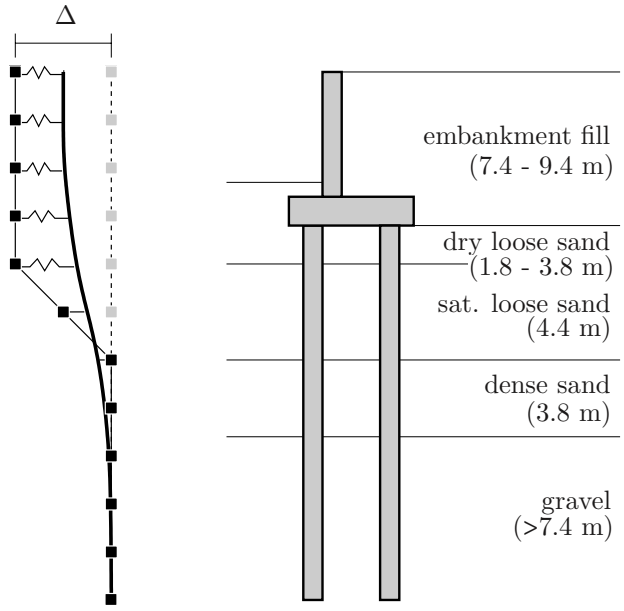

Figure 3.9: Applied displacement profile for equivalent shaft BNWF model of Puente Mataquito southwestern abutment.

In the current work, the unmodified and running average values are both considered in order to assess how each definition affects the compatible force-displacement state determined at the end of the procedure.

3.1.10 Slope Stability and Deformation Analysis

The slope stability model is used to compute the horizontal resisting force required at the center of the liquefiable loose sand layer to reach a factor of safety FS = 1.0 for a series of horizontal accelerations. As discussed in Section 3.1.7, several configurations of this model are considered in order to assess the sensitivity of the results to different modeling decisions. Table 3.3 shows the foundation resisting force values determined for each slope stability analysis approach (Bishop, 1955; Janbu, 1973) with various model parameters.

As expected, using a variable strength in the liquefiable layer or a non-zero deck resistance requires less foundational resistance to achieve FS = 1.0 than the corresponding cases with constant S_u or $F_{\text{deck}} = 0$. An interesting aspect of the results in Table 3.3 is that the choice of analysis method makes a significant difference in the stabilizing force returned for a given yield acceleration. In general, the Janbu approach returns larger forces for a given combination of k_y, F_{deck}, and S_u than those computed using the Bishop approach.

Table 3.3: Foundation resisting forces (in kN/m) necessary to reach FS = 1.0.

	constant S_u				varying S_u			
	$F_{\text{deck}} = 0$		$F_{\text{deck}} = 377$ kN/m		$F_{\text{deck}} = 0$		$F_{\text{deck}} = 377$ kN/m	
k_y (g)	Bishop	Janbu	Bishop	Janbu	Bishop	Janbu	Bishop	Janbu
0.05	25	136	45	0	0	42	45	0
0.10	192	403	55	38	0	88	46	0
0.15	426	716	223	340	65	344	48	0
0.20	697	1047	476	695	290	649	87	272
0.25	973	1321	747	1039	571	996	339	619
0.30	1229	1693	1025	1325	865	1341	624	986
0.35	1511	1884	1286	1643	1216	1639	919	1352
0.40	1913	2201	1602	1911	1627	1982	1314	1651

With $F_{\text{deck}} = 377$ kN/m, the passive force of fill acting over the depth of the bridge deck, the Bishop approach appears to have issues at lower yield accelerations, especially for the variable S_u cases, as the required resisting forces are larger than for $F_{\text{deck}} = 0$.

The displacements necessary for determination of the compatible state for the foundation are estimated using a Newmark rigid sliding block approach for each considered acceleration value. The predictive model of Bray and Travasarou (2007) is used for this purpose. Using this model, the nonzero displacement d in centimeters can be estimated for the Newmark rigid sliding block case as

$$\begin{aligned}\ln(d) = &-0.22 - 2.83\ln(k_y) - 0.333(\ln(k_y))^2 + 0.566\ln(k_y)\ln(\text{PGA}) \\ &+ 3.04\ln(\text{PGA}) - 0.244(\ln(\text{PGA}))^2 + 0.278(M-7) \pm \epsilon \end{aligned} \tag{3.7}$$

where PGA is the peak ground acceleration of the ground motion, M is the moment magnitude of the event, and ϵ is a normally distributed random variable with zero mean and a standard deviation of 0.66. The variability in this estimated displacement is considered by computing the 16 and 84% exceedance values from (3.7), thus establishing a range of estimated displacement values for each foundation resisting force. Because the standard deviation for the natural logarithm of displacement is 0.66, these values are computed as as $d_{16\%} = \exp(d - 0.66)$ and $d_{84\%} = \exp(d + 0.66)$, respectively. Table 3.4 lists the 16%, mean, and 84% displacements estimated from (3.7) using the magnitude, $\text{M}_w = 8.8$, and peak ground acceleration, PGA = 0.4 g, of the 2010 Maule event.

Table 3.4: Displacements estimated using Bray and Travasarou (2007) procedure.

k_y (g)	$d_{16\%}$ (cm)	d (cm)	$d_{84\%}$ (cm)
0.05	42.0	80.9	155.9
0.10	13.8	26.8	51.6
0.15	3.9	10.9	22.3
0.20	0.0	3.3	9.8
0.25	0.0	0.0	3.8
0.30	0.0	0.0	0.0
0.35	0.0	0.0	0.0
0.40	0.0	0.0	0.0

3.1.11 Determination of Compatible Force-Displacement State

The foundation displacement used for design purposes is determined by finding the compatible state indicated by the initial foundation pushover and slope stability/deformation analyses. This is accomplished by plotting the force-displacement data returned from each analysis type and noting the intersection of the two curves. The foundation resisting force values determined in the slope stability analysis represent the resisting force per unit width of soil, thus, in order to compare the two data sets, the shear force values computed in the pushover analysis must be divided by an appropriate width. Two widths are considered for this purpose, the embankment crest width, $w = 12.4$ m, taken from the actual geometry at Puente Mataquito, and the tributary embankment width, $w_t = 19.9$ m, computed per the recommendations of Boulanger et al. (2006).

Figure 3.10 shows the compatibility plots for pushover curves defined with both the running average and unmodified shear forces, V_{run} and V_{unmod}, respectively, scaled by w and w_t and slope stability/deformation curves computed using the Janbu method with overburden dependent strength in the liquefiable layer and $F_{\text{deck}} = 377$ kN/m. The curve for the mean displacement, d, is shown as a solid line, and the $d_{16\%}$ and $d_{84\%}$ curves are shown as dashed lines. The compatible states resulting from the same set of parameters, but with the Bishop method of slope stability analysis, are shown in Figure 3.11. These plots represent only a portion of the considered cases, however, they provide and example of how the compatible state is determined for actual data, and demonstrate the variability of the compatible state for a series of modeling decisions. Tables 3.5 and 3.6 provide

the compatible displacement values determined for each considered combination of model parameters. The maximum values for $F_{\text{deck}} = 0$ and $F_{\text{deck}} \neq 0$ and the minimum overall value are highlighted. The boxed values represent the range of displacements corresponding to the modeling decisions recommended by Martin et al. (2002) as modified by Boulanger et al. (2006) and Ashford et al. (2011).

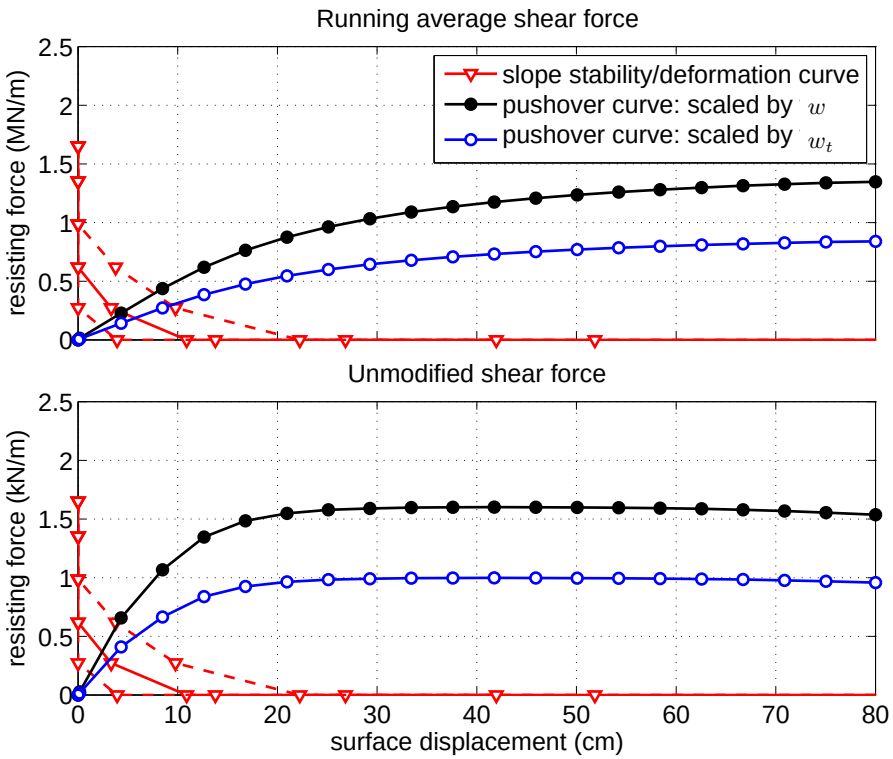

Figure 3.10: Compatible force-displacement states using the Janbu (1973) method for slope stability analysis with a varying S_u in the liquefied layer and $F_{\text{deck}} = 377$ kN/m.

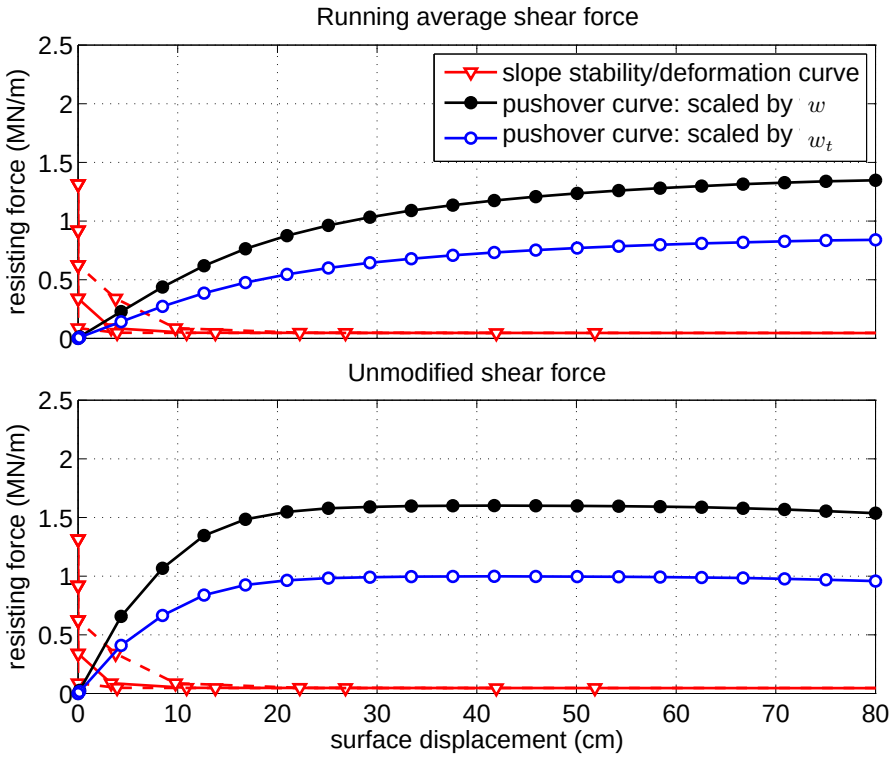

Figure 3.11: Compatible force-displacement states using the Bishop (1955) method for slope stability analysis with a varying S_u in the liquefied layer and $F_{\text{deck}} = 377$ kN/m.

Table 3.5: Compatible displacements (in cm) for various pushover and slope stability/deformation curves using the method of Janbu (1973).

16^{th} percentile displacements – $d_{16\%}$

	$F_{\text{deck}} = 0$		$F_{\text{deck}} = 377$ kN/m	
pushover curve	constant S_u	varying S_u	constant S_u	varying S_u
V_{run}/w	10.3	5.7	5.6	2.2
V_{run}/w_t	13.6	7.7	7.3	2.6
V_{unmod}/w	4.7	2.8	2.9	1.2
V_{unmod}/w_t	7.5	3.8	3.8	1.7

mean displacements – d

	$F_{\text{deck}} = 0$		$F_{\text{deck}} = 377$ kN/m	
	constant S_u	varying S_u	constant S_u	varying S_u
V_{run}/w	13.8	8.5	8.7	4.4
V_{run}/w_t	20.2	11.0	10.9	5.7
V_{unmod}/w	6.8	4.1	4.3	2.4
V_{unmod}/w_t	10.3	6.3	6.5	3.1

84^{th} percentile displacements – $d_{84\%}$

	$F_{\text{deck}} = 0$		$F_{\text{deck}} = 377$ kN/m	
	constant S_u	varying S_u	constant S_u	varying S_u
V_{run}/w	18.6	12.1	12.6	7.6
V_{run}/w_t	29.2	16.8	17.2	9.4
V_{unmod}/w	8.8	6.3	6.6	4.0
V_{unmod}/w_t	15.5	9.1	9.5	5.8

Table 3.6: Compatible displacements (in cm) for various pushover and slope stability/deformation curves using the method of Bishop (1955).

16th percentile displacements – $d_{16\%}$

	$F_{\text{deck}} = 0$		$F_{\text{deck}} = 377$ kN/m	
pushover curve	constant S_u	varying S_u	constant S_u	varying S_u
V_{run}/w	6.9	2.6	4.2	1.3
V_{run}/w_t	9.4	3.2	5.9	2.0
V_{unmod}/w	3.2	1.4	2.2	0.5
V_{unmod}/w_t	4.4	1.9	3.0	0.8

mean displacements – d

	$F_{\text{deck}} = 0$		$F_{\text{deck}} = 377$ kN/m	
	constant S_u	varying S_u	constant S_u	varying S_u
V_{run}/w	9.4	4.7	6.9	2.6
V_{run}/w_t	13.1	6.3	9.0	3.1
V_{unmod}/w	4.4	2.4	3.2	1.5
V_{unmod}/w_t	6.9	3.2	4.7	2.0

84th percentile displacements – $d_{84\%}$

	$F_{\text{deck}} = 0$		$F_{\text{deck}} = 377$ kN/m	
	constant S_u	varying S_u	constant S_u	varying S_u
V_{run}/w	12.9	7.6	9.6	5.3
V_{run}/w_t	18.6	9.5	13.4	6.7
V_{unmod}/w	6.3	3.8	4.8	2.7
V_{unmod}/w_t	9.5	5.6	7.3	3.7

There is significant variability in the compatible displacements for the different combinations of slope stability modeling decisions and pushover curve definition techniques. Estimated displacements range from 0.5 to 29.2 cm over the full spectrum of considered cases, and from 0.5 to 17.2 cm for those cases that consider the resistance provided by the bridge deck. This variability is apparent within the context of the boxed values in Tables 3.5 and 3.6, which range from 3.1 to 10.9 cm. Even if the scope of the study is restricted to the mean displacement cases with overburden dependent strength for the liquefied layer, as shown in Figures 3.10 and 3.11, there is variability depending on the particular slope stability analysis procedure used in the slope stability/deformation analysis.

Figures 3.12 shows the compatibility plot for all of the considered cases and 3.13 shows the compatibility plot for only the $F_{\text{deck}} \neq 0$ cases. The shaded portions of these plots represent the range of compatible displacements implied by the application of the procedure to the Puente Mataquito southwest abutment foundation and approach embankment. It is not practical to assess the foundation performance at all of the compatible states shown in these plots, however, a range of structural demands can be obtained through consideration of the minimum and maximum estimated displacements, and the average structural demands can be estimated by defining an average compatible displacement value. In order to determine a single displacement that is representative of each data set, the centroid of the shaded areas defined in the compatibility plots are computed and plotted as solid dots in Figures 3.12 and 3.13. The average displacement states computed with this approach are 11.4 cm for the full data set and 7.5 cm for the $F_{\text{deck}} \neq 0$ cases. The latter value corresponds well with the boxed displacement values of Tables 3.5 and 3.6.

3.1.12 Assessment of Foundation Performance

With a range of compatible displacements defined using the results of the initial pushover and slope stability/deformation analysis phases, the final step in the pile-pinning analysis procedure is the assessment of the foundation performance at the compatible displacement. This is accomplished using a pushover analysis with the equivalent shaft BNWF model where the applied surface displacement is set equal to the minimum, average, and maximum

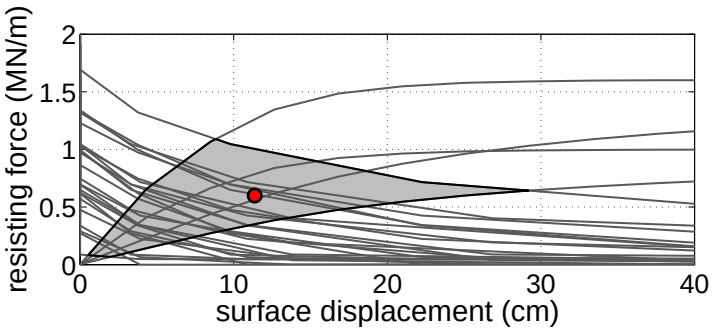

Figure 3.12: Variability in compatible state for all considered cases.

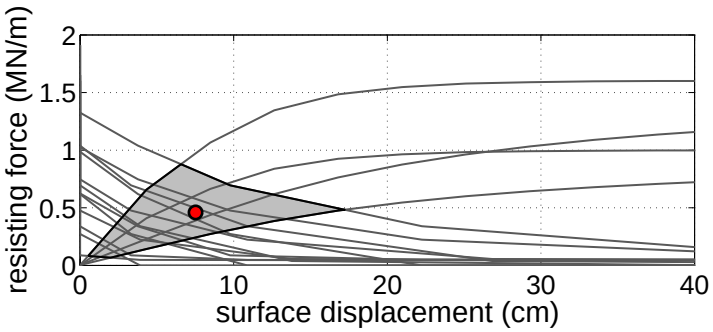

Figure 3.13: Variability in compatible state for cases with $F_{\text{deck}} \neq 0$

compatible displacement values discussed in the previous section and shown in Figures 3.12 and 3.13. Consideration of these values defines a range of estimated foundation demands that can be compared to the observed site displacements as well as the results of the 3D foundation model.

The shaft displacement profiles, shear force diagrams, and bending moment diagrams resulting from lateral spreading pushover analyses of the BNWF model for each considered surface displacement are shown in Figures 3.14 and 3.15. The shear forces and bending moments in these plots are average shaft values computed by dividing the demands returned by the equivalent foundation model by the number of shafts in the group. As expected, the wide range of compatible displacements results in a wide range of estimated foundation demands, with larger applied displacements leading to larger shear and moment demands. Table 3.7 provides the maximum shaft displacement, shear force, and bending moment returned by the foundation model for each compatible displacement value.

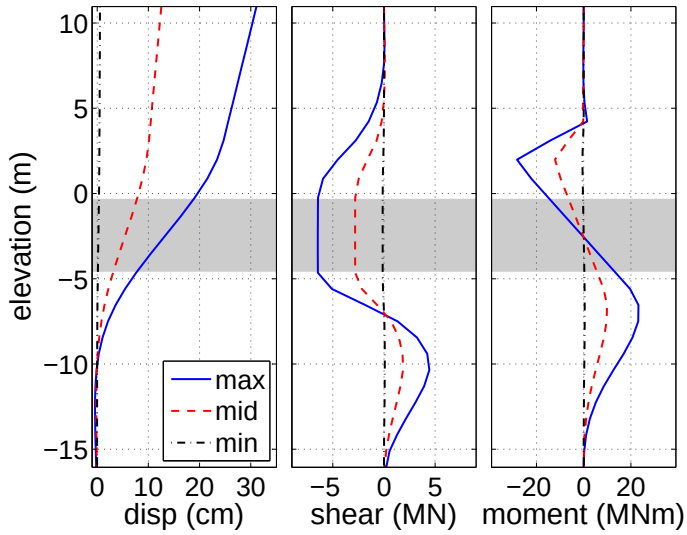

Figure 3.14: Shaft displacement, shear, and moment demands for minimum (0.5 cm), mean (11.4 cm), and maximum (29.2 cm) compatible states for full data set.

Aside from the 0.5 and 7.5 cm cases, the maximum moments returned from this study are in excess of the 9.0 MN·m design capacity for the Puente Mataquito shaft foundations. Of the considered displacements, the average for the $F_{\text{deck}} \neq 0$ cases, 7.5 cm, is the most representative of the recommendations of Martin et al. (2002), Boulanger et al. (2006), and Ashford et al. (2011). It is encouraging that the foundation performance for this displacement correlates at least roughly with the observed foundation performance under lateral spreading. Observations at the southwest abutment indicated little or no lateral displacement of the abutment, which suggests that the shafts were able to restrain the movement of the foundation while remaining primarily in the elastic regime. For a 7.5 cm applied displacement, the BNWF model suggests shaft performance in line with the likely foundation behavior, with the shafts approaching but not reaching the plastic moment capacity. The estimated and reported abutment displacements are not in direct agreement, however, the estimated displacement is small enough for the bridge to have experienced while sustaining little visible damage.

The discrepancy between the foundation demands for the average displacements resulting from full data set and the $F_{\text{deck}} \neq 0$ data set highlights the importance of the lateral

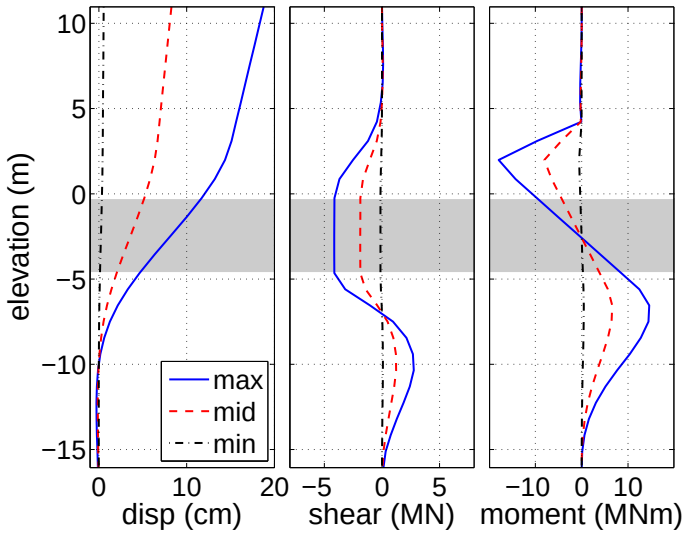

Figure 3.15: Shaft displacement, shear, and moment demands for minimum (0.5 cm), mean (7.5 cm), and maximum (17.2 cm) compatible states for $F_{\text{deck}} \neq 0$ data set.

Table 3.7: Maximum shaft displacement, shear, and moment demands for five considered compatible soil displacement states.

compatible disp	max disp (cm)	max shear (MN)	max moment (MN·m)
0.5 cm	0.55	0.13	0.54
7.5 cm	8.3	1.88	8.06
11.4 cm	12.5	2.82	12.11
17.2 cm	18.8	4.14	17.92
29.2 cm	31.1	6.47	28.20

resistance provided by the bridge deck in determining the foundation response to the kinematic demands of lateral spreading. This is evident in the results of this analysis, as the inclusion or omission of F_{deck} in the slope stability analysis phase significantly changes the compatible displacement state, and is confirmed by the results from the 3D model of the southwest abutment discussed in the following sections. The inclusion of the bridge deck resistance as a constant force equal to the full passive resistance of soil acting over the area of the deck is a convenient approach, but the full passive force may not develop for all displacements and this practice may overestimate the lateral resistance provided by the bridge deck. Additionally, other site-specific factors may affect the available lateral deck resistance. Expansion gaps are typically included at the connection of the deck to the abutment, and

a certain amount of displacement must occur before significant deck resistance is available. It is also possible for the deck to become unseated at larger displacements and, as discussed by Franke (2011), the factors leading to this response are obscure, as similarly constructed bridges have displayed opposing deck behavior for similar lateral spreading demands.

Further research is necessary to fully understand all of the factors contributing to the available deck resistance during lateral spreading, however, there are simpler approaches that can be incorporated into the pile pinning analysis procedure to consider the uncertainty in the contribution of the deck resistance to the compatible displacement for the foundation. One such approach is the use of a running average shear force in the definition of the pushover curve as proposed by Boulanger et al. (2006). The use of this technique adds some conservatism to the final result by lowering the pushover curve, which returns a larger compatible displacement than would be estimated for an unmodified shear force. Another approach is the consideration of multiple compatible states for which F_{deck} is set to both zero and nonzero values. The pushover and slope stability analyses used in this design procedure are relatively inexpensive in terms of time and computational effort, therefore, performing them multiple times is feasible in practice. The range of compatible displacements resulting from this approach can be used to determine a final displacement estimate, perhaps similar to the centroidal approach discussed above, or to define a range of foundation demands for use in design. More details on the Mataquito bridge and a complete comparison study using this simplified design approach and 3D numerical simulations can be found in (Arduino et al., 2017)

3.2 Unrestrained Case: Llacolén Bridge

The 2160 m long Llacolén bridge spans the Bío Bío river between the cities Concepción and San Pedro de la Paz. The superstructure, consisting of four traffic lanes and pedestrian sidewalks, is supported by column bents with inverted-T cap beams, which in turn carry the loads from simply-seated, prestressed I-girders forming the deck of the bridge.

Figure 3.16: Lateral spreading and span collapse of northeast approach embankment to Llacolén Bridge (FHWA, 2011).

During the Maule earthquake, the eastern bank of the Bío Bío river experienced an extensive amount of lateral spreading due to liquefaction. The northeastern approach of the Llacolén bridge was reported to experience about 25 cm of lateral displacement towards the river and 40 cm of settlement. As a result, the approach span of the bridge was unseated while the westbound entrance came very close to collapse, Figure 3.16. Other than the collapse of the northeastern span, the remaining parts of the bridge remained operable.

The Llacolén bridge fits the case where three-dimensional soil effects are not applicable. Therefore, following the Caltrans (2011) procedure for unrestrained ground displacement case presented in Section 2.1.2, the pile pinning model of the northeast approach is created. Similar to the previous case, the purpose for development of this model is to assess the viability of this design procedure through comparison with the observations made at the bridge site and results of the 3D finite element models (Arduino et al., 2017). Therefore

a BNWF model of the foundation is developed using a representative shaft model and definition of p-y curves that appropriately captures the soil-shaft interaction for the idealized soil profile, liquefied layer and group effects.

3.2.1 Development of Idealized Soil Profile

Subsurface information available at the Llacolén bridge site are two series of pre-event Standard Penetration Test (SPT) blow counts and the information gathered after the event by reconnaissance teams and other institutes. First series of pre-event tests were conducted by the Japanese International Cooperation Agency (JICA) in 1993 at four locations along the bridge alignment. A consultant consortium of Systra-Sofretu/Cade Idepe performed six additional standard penetration tests in 1996. Using this information an idealized soil profile is obtained to be used in the development of the numerical models of the Llacolén bridge's northeast bent. Figure 3.17b shows a longitudinal profile of the subsurface strata along the bridge axis and the location of the pre-event SPT experiments. Although boring logs are not available for deeper soils at the site, boring logs at the adjacent bridge, Puente Juan Pablo II, indicate that the soil profile is generally non-plastic and cohesionless. For the purposes of the numerical models, minor variations in the soil profile are ignored and all materials are assumed to be cohesionless. The groundwater table is assumed to be at the average annual level of the river flow and all of the soil below the groundwater table is assumed to be saturated.

Based on the available subsurface information, the profile can be divided roughly into four soil layers, an upper loose sand layer, a middle layer of denser sand over a layer of medium dense sand and an underlying dense gravel layer. A weighted average SPT resistance value is calculated for each layer from the available data. Representative friction angles, ϕ, for each layer are estimated from the SPT values using the correlation proposed by Kulhawy and Mayne (1990). Estimated properties for the site soils are summarized in Table 3.8.

Table 3.8: Model properties for soil layers in idealized soil profile.

Soil Type	ρ (Mg/m^3)	ϕ (°)	$G_{\max}$ (MPa)	$K_{\max}$ (MPa)	e	ϕ_{pt} (°)
Loose sand	1.7	33	10.3	30.8	0.77	29
Dense sand	2.0	35	20.5	44.4	0.65	26
Med. dense sand	1.8	32	10.3	26.7	0.77	26
Gravel	2.1	42	41.0	80.0	0.55	26

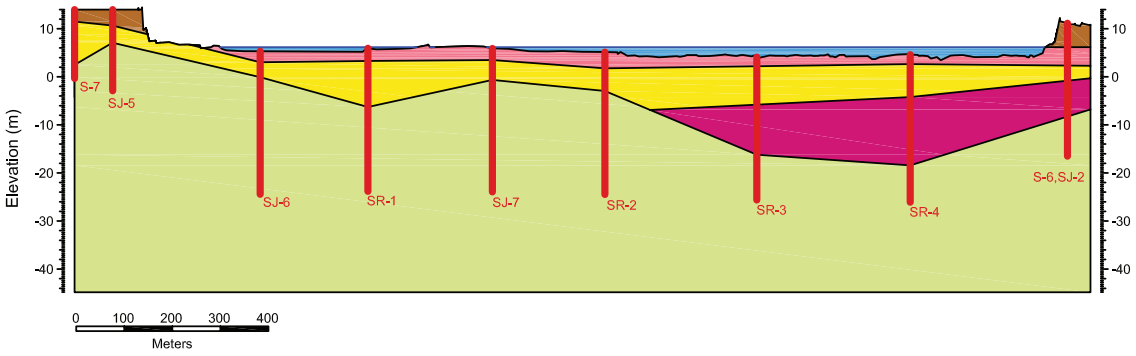

(a) Elevation view of the idealized soil profile with the location of SPT locations.

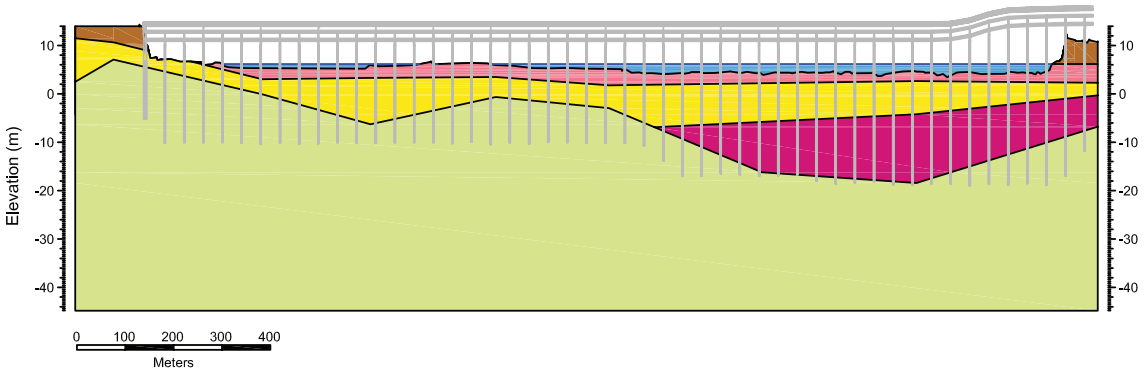

(b) Elevation view of the idealized soil profile with the longitudinal view of the bridge.

Figure 3.17: Elevation view of the idealized soil profile along with the location of SPT boreholes and the longitudinal bridge profile (Vertical scale increased).

3.2.2 Liquefaction Potential Assessment

Susceptibility of the soil to liquefaction at the Llacolén bridge site is assessed using the procedure proposed by Youd et al. (2002). The nearest available ground motion to Llacolén bridge site recorded a peak ground acceleration (PGA) of 0.65 g (Boroschek et al., 2010). Based on the available grain size distribution data for the upper parts of the soil profile, fines content fall in the range of 5% to 33%. An SPT resistance of 26 is shown to be the threshold value indicating if a soil in this site is susceptible to liquefaction. Based on this analysis, the saturated portion of the upper loose sand layer is shown to be susceptible to liquefaction. The assessment procedure by Youd et al. is only valid up to depths of 15 meters. Therefore the points below 15 meters are not considered in this analysis although they might be subject to liquefaction. This assumption is not necessarily representative of actual conditions at the Llacolén bridge site but for the purposes of this research is acceptable.

3.2.3 Foundation Modeling Approach

Foundation shafts and pier columns are modeled taking the same approach as explained in Section 3.1.3. As shown in Figure 3.18, the pier consists of 11 columns and an inverted-T beam on which the girders are seated. This beam is modeled with displacement-based beam-column elements using properties that are calculated based on the geometry of the beam. The same type of element is used to model the columns and foundation shafts. Pier columns are made of 1.35^{m} circular sections with two different reinforcement layout (Figure 3.19a). The moment-curvature behavior of these sections under the assumed axial force is shown in Figure 3.20a. The foundation shafts are 1.5^{m} diameter circular sections with four different types of reinforcement arrangement(Figure 3.19b). Figure 3.20b depicts the moment-curvature diagrams of each of these sections.

The bridge deck geometry is not explicitly modeled in the numerical models, instead a linear elastic spring is used to represent the effects of the presence of the bridge deck. The constitutive behavior of the spring considers the existence of a gap which when closed acts in compression. The spring considers zero tensile and compressive stiffness if the gap is

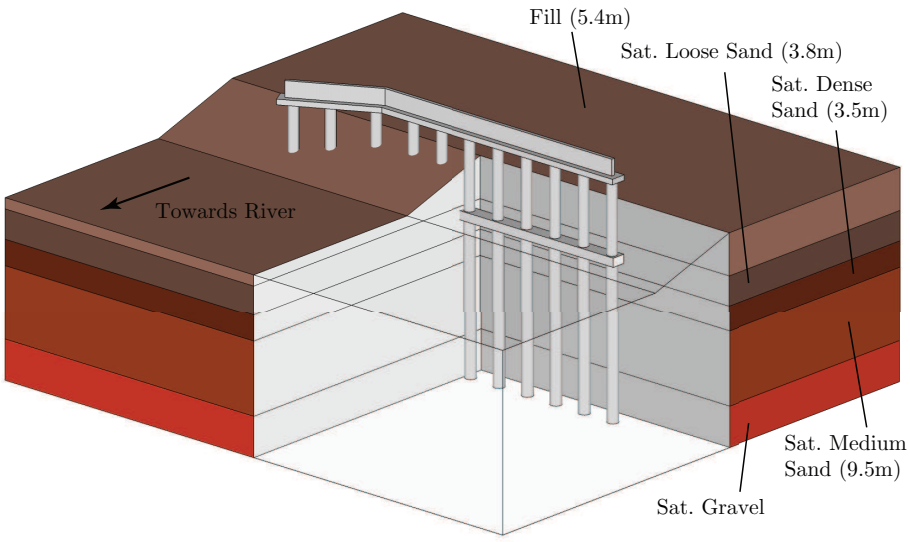

Figure 3.18: Schematic of the northeast approach of the Llacolén bridge with the idealized soil profile.

open. Based on the deck geometry and the reinforcement details of the deck, a gross cross-sectional area and a composite stiffness can be calculated for the bridge deck. Assuming a smeared reinforced concrete elastic modulus of $E_{deck} = 63.2^{\text{GPa}}$, and using the span length of 21 meters, a stiffness of $k = EA/L$ can be calculated for the deck spring. Assuming equal tributary area for each of the pier columns, the area A is divided by the number of columns and a spring is defined for each column. These springs are connected to the head of the columns on one side and are assumed fixed in the other side. The gap is assumed to be almost equal to the sum of the openings of the expansion joints on each side of the pier which is 10^{cm}.

3.2.4 Development of Foundation Model

The northeast approach pier foundation consists of 11 piles located side-by-side, 3 diameters apart and tied together with a cap beam. The cap beam is located in the liquefiable layer and is not likely to provide much resistance to lateral spreading. Each pile is made of reinforced concrete with 4 different reinforcement arrangement along their length resulting

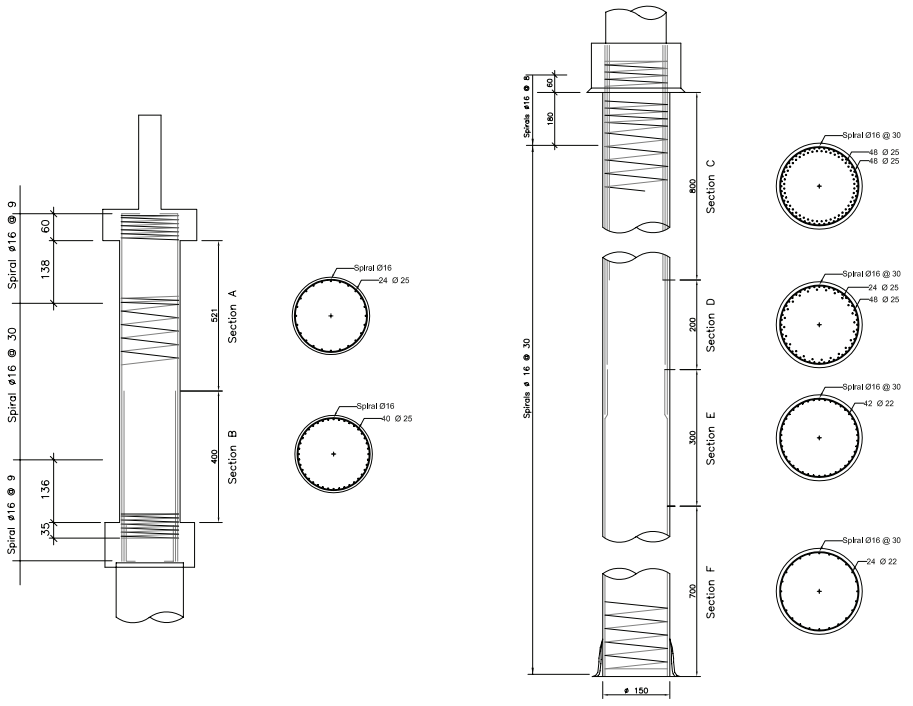

(a) (b)

Figure 3.19: Construction detail of the Llacolén bridge foundation shafts and pier columns.

in 4 sections with different capacities and moment-curvature diagrams. The approach bent is made of 11 pier columns which are partly embedded and each consist of 2 different sections (Figure 3.20). The moment-curvature diagrams of these sections are scaled per Caltrans recommendations to convert the foundation system into an equivalent shaft.

Both linear elastic shaft response and nonlinear inelastic shaft response are considered and a separate model is created for each case. The properties for the linear elastic shaft are determined using the initial bending stiffness seen in the moment-curvature plots of Figure 3.20, and geometry of the sections. For a single pier column section the initial bending stiffness is $EI = 3.473\text{GN.m}^2$ which along with the gross second moment of area for a single shaft, $I_g = 0.163\text{m}^4$, results in an elastic stiffness $E = 21.3\text{GPa}$. Assuming a Poisson's ratio of 0.25, this elastic stiffness gives a shear modulus of $G = 8.52\text{GPa}$. These values for the foundation piles are $EI = 4.722\text{GN.m}^2$, $I_g = 0.249\text{m}^4$ resulting in $E = 19.0\text{GPa}$ and

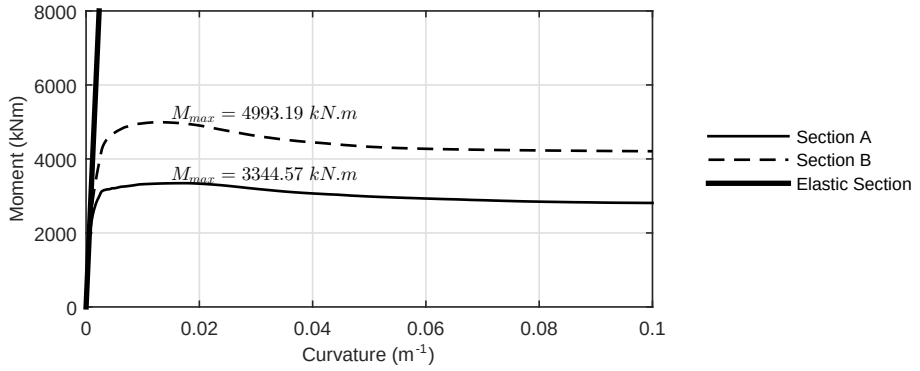

(a) Pier column sections A and B.

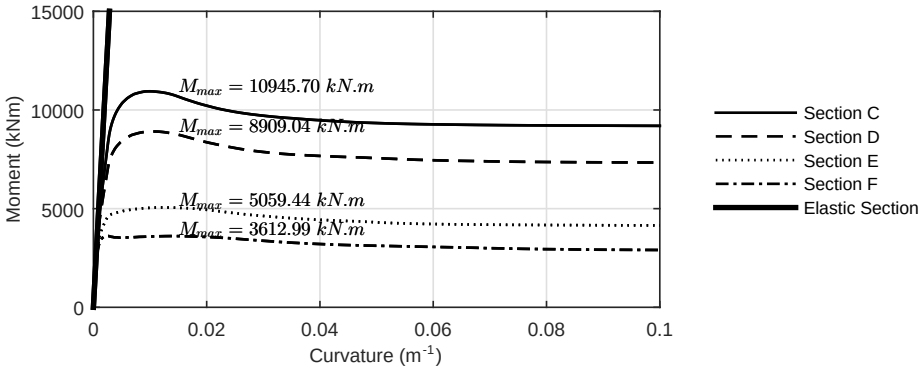

(b) Foundation pile sections C, D, E and F.

Figure 3.20: Model moment-curvature response for different sections of the Llacolén bridge foundation pile and pier column at design axial force. Equivalent elastic section stiffness is shown as initial tangent to moment-curvature response.

$G = 7.6$GPa. Table 3.9 presents a summary of the linear elastic equivalent shaft properties. The moment-curvature diagrams of single nonlinear shaft sections are scaled by the number of piles in the group.

Since the group of piles in the northeast approach of Llacolén bridge is a side-by-side arrangement except for the 3 northern piles that are located eccentric to the group axis, no rotational spring is considered in the BNWF analyses to represent the rotational stiffness due to group effects. Eccentricity of the northern 3 piles introduces some local rotational stiffness however it is assumed that this stiffness is negligible compared to global response of the bridge bent.

Table 3.9: Properties of linear elastic equivalent beam model for grouped shaft foundation.

	Parameter	Single Shaft	Equivalent Shaft
Pier Columns	E	21.3 GPa	21.3 GPa
	I	0.163 m^4	1.793 m^4
	A	1.431 m^2	15.745 m^2
	G	8.52 GPa	8.52 GPa
Foundation Piles	E	19.0 GPa	19.0 GPa
	I	0.249 m^4	2.734 m^4
	A	1.767 m^2	19.439 m^2
	G	7.6 GPa	7.6 GPa

A linear compressional spring is used at the column head to represent the existence of the bridge deck. This spring incorporates a gap, before which closure no force is exerted to the foundation system. As the gap is closed, the spring acts in compression and simulates a linear elastic deck section. Stiffness of this spring is calculated using the elastic properties of the deck and its geometry.

3.2.5 Definition of p-y curves

Soil-pile interaction in BNWF analysis is represented through series of p-y curves defined based on the idealized soil profile. Necessary parameters to define these curves are the ultimate lateral resistance, p_u, and initial stiffness, k_T. Four distinct methods for calculation of p_u based on the idealized soil profile properties are used here: (1) method by Broms (1964), (2) method by Fleming et al. (1985), (3) method by Brinch Hansen (1961) and (4) method by API (1987). Figure 3.21 shows the calculated values of p_u for each of these methods along with the reduced values due to the presence of a liquefiable layer as recommended by McGann et al. (2012). Although there is a great discrepancy among the values of p_u calculated using each of these methods especially at depth, since most of the deformations happen close to the surface, the results are less impacted by the variance of p_u values.

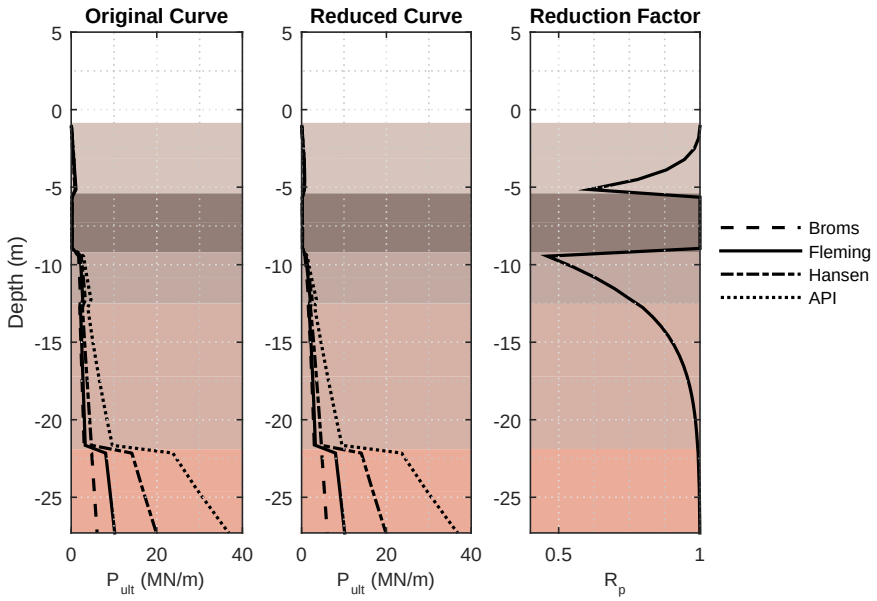

Figure 3.21: Calculated p_u for definition of p-y curves. Effects of liquefied soil layer on neighboring layers p_u is applied based on the procedure proposed by McGann et al. (2012).

API (1987) presents an empirical relationship for the initial stiffness, k_T, of $p-y$ curves. Another method for calculating this parameter is using the modulus reduction of the idealized soil material and relating the strain at which the shear stiffness is reduced to half the original value, γ_{50}, to ϵ_{50} which is the strain at which half the strength is mobilized in a conventional triaxial compression test. Then the initial stiffness is calculated using the semi-empirical equation $y_{50} = 2.5D\epsilon_{50}$ and the definition of the p-y curve, where y_{50} is the displacement at which half the p_u is mobilized and D is the pile diameter. Figure 3.22 illustrates the comparison between these two methods along with the reduced curves as proposed by McGann et al. (2012).

Caltrans (2011) recommends group efficiency factors of Mokwa and Duncan (2001) to incorporate the loss of efficiency of piles due to group effects. However this procedure is less applicable to side-by-side pile groups where only one row of piles exist. For side-by-side pile

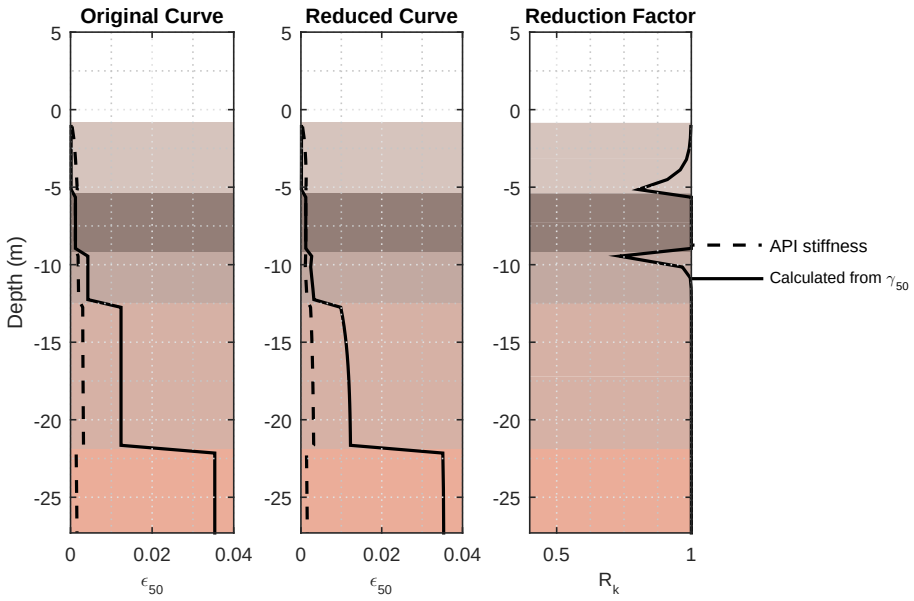

Figure 3.22: Comparison of the ϵ_{50} values based on the stiffness proposed by API and calculated based on γ_{50}, Effects of liquefied soil layer on neighboring layers ϵ_{50} is applied based on the procedure proposed by McGann et al. (2012).

groups, Reese and Van Impe (2010) suggests using an efficiency factor of

$$e = \begin{cases} 0.64\,(s/D)^{0.34} & 1 \leq s/D \leq 3.75 \\ 1.0 & s/D \geq 3.75 \end{cases}$$

where s is the spacing between the piles. The group effect p-multiplier for the equivalent shaft model is computed as the product of number of piles with the group efficiency factor

$$p_{group} = 11 \times 0.93 = 10.23$$

The residual strength of the liquefiable soil is computed using the undrained shear strength hybrid expression presented by Kramer (2008) per Caltrans recommendation

$$S_{ur} = 2116 \exp\left(-8.444 + 0.109(N_{1,60}) + 5.379\left(\frac{\sigma'_v}{2116}\right)^{0.1}\right)$$

Table 3.10: Displacements estimated using Bray and Travasarou (2007) procedure.

k_y (g)	$d_{16\%}$ (cm)	d (cm)	$d_{84\%}$ (cm)
0.05	88.7	171.6	332.1
0.1	35.8	69.3	134.0
0.15	18.1	35.1	67.9
0.2	10.5	20.3	39.3
0.25	6.6	12.8	24.7
0.35	3.1	6.0	11.5
0.45	1.7	3.2	6.2
0.55	1.0	1.9	3.7
0.65	0.6	1.2	2.3

where S_{ur} is the undrained shear strength, σ'_v is the vertical effective stress, and $N_{1,60}$ is the corrected SPT blow count. For $N_{1,60} = 10$ and $\sigma'_v = 106^{\text{kPa}}$, the undrained shear strength of the liquefiable layer is computed equal to $S_{ur} \approx 15^{\text{kPa}}$.

3.2.6 Deformation Analysis

Ground crust displacement due to liquefaction of the subterranean layers is needed to define the displacement profile resulting in lateral spreading. (Caltrans, 2011) recommends using either the Newark-based method by Bray and Travasarou (2007) or the procedure by Faris et al. (2006) which is based on strain potential. Estimated ground displacements using the expression presented by Bray and Travasarou (2007)

$$\begin{aligned}\ln(d) = &- 0.22 - 2.83\ln(k_y) - 0.333(\ln(k_y))^2 + 0.566\ln(k_y)\ln(\text{PGA}) \\ &+ 3.04\ln(\text{PGA}) - 0.244(\ln(\text{PGA}))^2 + 0.278(M-7) \pm \epsilon \end{aligned} \tag{3.8}$$

using a peak ground acceleration, PGA $= 0.65g$ and moment magnitude, $M = 8.8$ are summarized in Table 3.10. The value of k_y needs to be estimated using some slope stability analysis method.

The second method by Faris et al. (2006) requires computation of the Displacement Potential Index (DPI) which is the integral of the strain potential within the liquefiable layer, that is $DPI = \int_{liq\ layer} \gamma_{max}\, dz$ where z is the depth measure. The amount of ground

deformation is then estimated as

$$d_{max}(m) = [DPI(m)]^{1.07}$$

Wu (2002) gives a relationship between $N_{1,60}$ and the estimated cyclic stress ratio, CSR, corrected for earthquake magnitude. Using a magnitude corrected CSR of 0.3 and a corrected SPT blow count of 10, this relationships results in a $\gamma_{max} = 0.36$. This results in a maximum ground displacement of $d = 140.0^{\text{cm}}$. Such large displacements mobilize the passive resistance of the soil completely and the structural demands become insensitive to the amount of displacement. Therefore a displacement of 100^{cm} is considered for the BNWF analyses.

3.2.7 Assessment of Foundation Performance

The final stage in pile-pinning analysis is applying the displacement profile to the equivalent BNWF model and assess the foundation performance under such loading conditions. Estimated p_u values using different methods result in slightly different foundation demands. Figure 3.23 shows the shaft displacement profile, shear force diagram and bending moment diagram resulting from lateral spreading pushover analysis of the BNWF model developed using each of the methods for estimating p_u values. In this figure a deck spring with a 10^{cm} gap is considered and initial stiffness of p-y curves are calculated using γ_{50}. This figure shows that BNWF results are relatively insensitive to the method chosen for definition of the ultimate lateral resistance of the p-y curves. Figure 3.24 depicts the effects of choosing initial stiffness using any of the two methods described previously. In this case no deck spring is considered to emphasize the effect of the choice of stiffness on the results. Behavior of the shafts are linear elastic in this case to remove any side effects caused by the nonlinear behavior of the shafts. The effects are relatively small and are even smaller in the case a 10^{cm} gap deck spring is considered. From this point on, all the presented results are from cases using p_u calculated from Brinch Hansen (1961) and initial stiffnesses calculated using γ_{50}.

Figure 3.25 compares BNWF results for linear elastic versus nonlinear cases and also

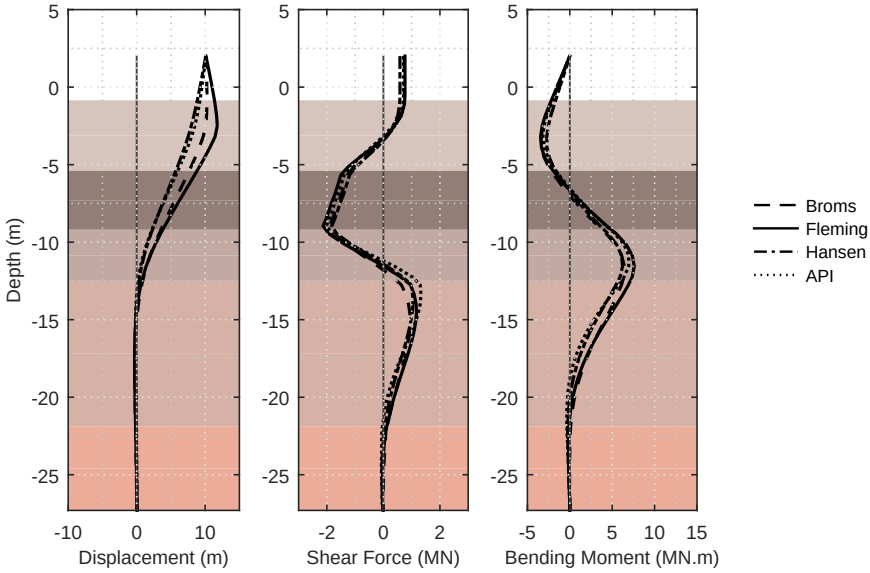

Figure 3.23: Effect of different p_u calculation methods on shaft bending demands at the end of analysis for 1-D BNWF model with 10^{cm} gap using back-calculated stiffness from γ_{50}.

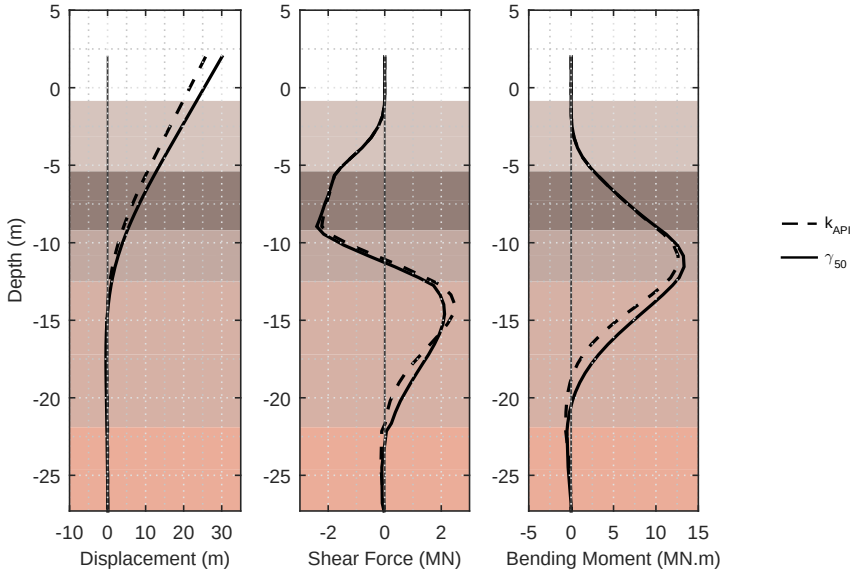

Figure 3.24: Effect of different initial stiffness calculation methods on shaft bending demands at the end of analysis for 1-D BNWF model with no deck using Hansen formulation.

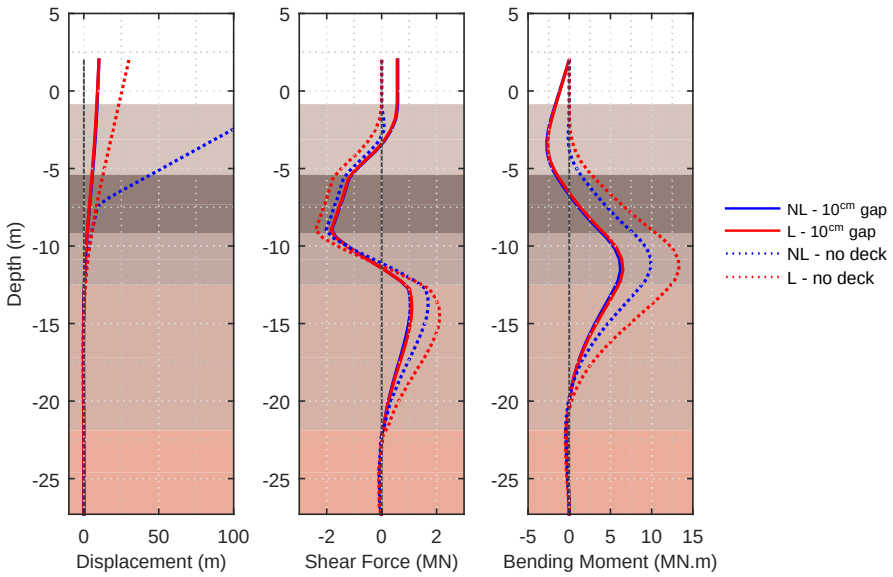

Figure 3.25: Effect of linear vs. nonlinear structural response on shaft bending demands at the end of analysis for 1-D BNWF model.

cases with a 10^{cm} gap deck versus cases with no deck considered. The importance of considering nonlinear behavior of the shafts is obvious since in the case with no deck, a plastic hinge is formed and the bending moments are redistributed. The shear force and bending moment diagrams are quite different in this case. However in the case where a deck spring is present, linearity of shaft behavior plays a less important role and there is no meaningful difference between them. In cases where a deck spring is considered the bending moment demands are different in nature. In these cases a negative moment demand is seen close to the surface due to the lateral force applied by the deck while decreasing the positive demands at depth.

The amount of lateral spreading observed in the bridge site is reported about 25^{cm}. Figures 3.26 and 3.27 depict the evolution of demand profiles with increasing free field displacements. It is obvious that at a 25^{cm} free field displacement the strength of the soil springs is fully mobilized close to the surface where most of the lateral spreading displacement profile exists. Comparing the result profiles from the case with no deck for 25^{cm} and 100^{cm} ground displacements, it is apparent that formation of the plastic hinge results in

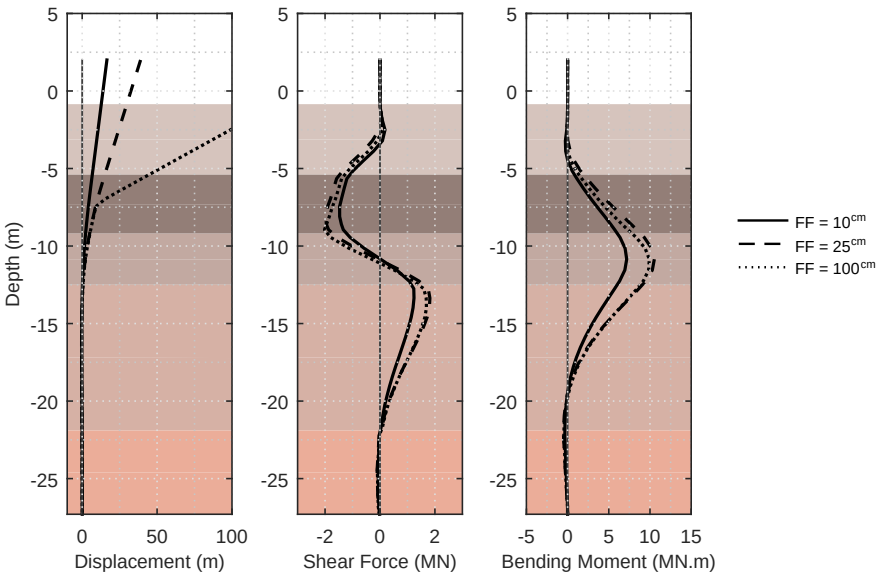

Figure 3.26: Effect of free field displacement on shaft bending demands for 1-D BNWF model with no deck.

redistribution of the bending moments. Figure 3.27 however shows that as soon as the deck gap is closed, further application of free field displacement has minimal effect on the structural demands. More details on the Llacolén bridge and a complete comparison study using this simplified design approach and 3D numerical simulations can be found in (Arduino et al., 2017)

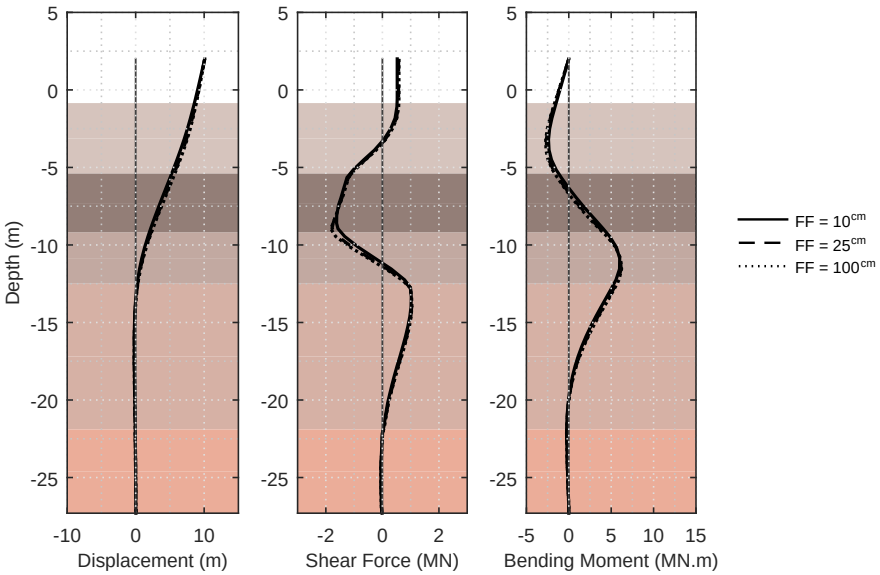

Figure 3.27: Effect of free field displacement on shaft bending demands for 1-D BNWF model with 10^{cm} gap.

Chapter 4

CONCLUSION

The design procedure used by the California Department of Transportation for bridge foundations subject to liquefaction-induced lateral ground deformation was reviewed to assess the state of current design practice for this load case.

The Caltrans procedure makes a distinction between cases for which it is expected that the foundation will provide lateral pinning resistance, and cases for which no resistance is assumed. For the cases where assuming foundational restraint appears to be reasonable, the pile pinning analysis procedure (Martin et al., 2002; Boulanger et al., 2006; Ashford et al., 2011), which is based on the assumption of compatibility between the foundation resistance and embankment deformation during lateral spreading, is adopted by Caltrans.

The pile pinning analysis procedure (Martin et al., 2002; Boulanger et al., 2006; Ashford et al., 2011) has been assessed through an application of the Caltrans (2011) version of the procedure to the southwest abutment of Puente Mataquito and the northeast approach of Llacolén bridge. In the case of Puente Mataquito the compatible displacements obtained from the pile pinning analysis were shown to possess great variability with respect to the particular assumptions and modeling choices made in the individual analysis phases that comprise the pile pinning approach. It was proposed that the compatible displacement used in the final foundation design phase be selected as an average of the compatible displacements resulting from a series of different modeling configurations and assumptions. In this manner, the design solution that is most representative of the site conditions can be obtained.

Pile pinning analyses were also performed for the Llacolén bridge to evaluate their credibility to be used for design in practice for a case where soil embankment three dimensional effects are not present. It was shown that if this method is applied carefully, with a careful estimation of ground displacement and correct definition of structural components in the

problem, e.g. the expansion gap and bridge deck resistance, they are able to predict the bending demands in foundations subject to lateral spreading loading conditions.

Appendix A

CONVERSION TABLE

Quantity	**From Metric Units**	**To English Units**	**Multiply by**
Length			
	km	mile	0.6214
	m	foot	3.2808
	m	inch	39.3701
Area			
	m^2	square foot	10.7639
	m^2	square inch	1550.0
Mass			
	kg	lb	2.2046
Mass density			
	kg/m^3	pcf	0.0624
Force			
	N	lb	0.2248
	kN	kip	0.2248
Pressure, stress, modules of elasticity			
	kPa	ksf	0.0209
	MPa	ksi	0.1450
Bending moment, torque, moment of force			
	kN·m	ft-kip	0.7376
Second moment of area			
	m^4	in^4	2402509.61
Velocity, speed			
	m/s	ft/s	3.2808
Acceleration			
	m/s^2	ft/s^2	3.2808

BIBLIOGRAPHY

American Association of State Highway and Transportation Officials (AASHTO) (2010a). *Guide Specifications for LRFD Seismic Bridge Design*. Washington, D.C., 1st edition.

American Association of State Highway and Transportation Officials (AASHTO) (2010b). *LRFD Bridge Design Specifications*. Washington, D.C., 5th edition.

American Petroleum Institute (API) (1987). *Recommended Practice for Planning, Designing and Constructing Fixed Offshore Platforms*. API Recommended Practice 2A(RP-2A), Washington, D.C., 17th edition.

American Petroleum Institute (API) (2007). *Recommended Practice for Planning, Designing and Constructing Fixed Offshore Platforms–Working Stress Design*. API Recommended Practice 2A-WSD (RP 2A-WSD), 21st edition. Errata and Supplement 3, October 2007.

Arduino, P., McGann, C., and Ghofrani, A. (2017). *Numerical evaluation of forces on piled bridge foundations in laterally spreading soil*. Washington State Department of Transportation (WSDOT).

Ashford, S. A., Boulanger, R. W., and Brandenberg, S. J. (2011). "Recommended design practice for pile foundations in laterally spreading ground." *PEER Report No. 2011/04*, Pacific Earthquake Engineering Research Center, University of California, Berkeley.

Bishop, A. W. (1955). "The use of the slip circle in the stability analysis of slopes." *Géotechnique*, 5(1), 7–17.

Boroschek, R., Soto, P., and León, R. (2010). *Registros del Terremoto del Maule, Mw=8.8, 27 de Febrero de 2010*. RENADIC Report 10/05.

Boulanger, R. W., Chang, D., Gulerce, U., Brandenberg, S. J., and Kutter, B. L. (2006). "Evaluating pile pinning effects on abutments over liquefied ground." *Seismic Performance and Simulation of Pile Foundations in Liquefied and Laterally Spreading Ground*, R. W. Boulanger and K. Tokimatsu, eds., GSP 145, ASCE. 306–318.

Boulanger, R. W., Kutter, B. L., Brandenberg, S. J., Singh, P., and Chang, D. (2003). *Pile Foundations in liquefied and laterally spreading ground during earthquakes: Centrifuge experiments and analyses*. Center for Geotechnical Modeling, University of California at Davis, Davis, CA. Rep. UCD/CGM-03/01.

Brandenberg, S. J., Boulanger, R. W., Kutter, B. L., and Chang, D. (2007a). "Liqufaction induced softening of load transfer between pile groups and laterally spreading crusts." *Journal of Geotechnical and Geoenvironmental Engineering, ASCE*, 133(1), 91–103.

Brandenberg, S. J., Boulanger, R. W., Kutter, B. L., and Chang, D. (2007b). "Static pushover analyses of pile groups in liquefied and laterally spreading ground in centrifuge tests." *Journal of Geotechnical and Geoenvironmental Engineering, ASCE*, 133(9), 1055–1066.

Bray, J. D. and Travasarou, T. (2007). "Simplified procedure for estimating earthquake-induced deviatoric slope displacements." *Journal of Geotechnical and Geoenvironmental Engineering, ASCE*, 133(4), 381–392.

Brinch Hansen, J. (1961). "The ultimate resistance of rigid piles against transversal forces." *Bulletin No. 12*, Geoteknisk Institute, Copenhagen, 5–9.

Broms, B. B. (1964). "Lateral resistance of piles in cohesionless soils." *Journal of the Soil Mechanics and Foundations Division, ASCE*, 90(SM3), 123–156.

California Department of Transportation (Caltrans) (2011). *Guidelines on Foundation Loading and Deformation Due to Liquefaction Induced Lateral Spreading*. Internal Policy Proposal, February 2011.

Faris, A. T., Seed, R. B., Kayen, R. E., and Wu, J. (2006). "A semi-empirical model for the estimation of maximum horizontal displacement due to liquefaction-induced lateral spreading." *Proceedings, 8th U.S. National Conference on Earthquake Engineering*, San Franciso, CA, April 18-22, Paper No. 1323.

Federal Highway Administration (FHWA) (1978). *Guidelines for Cone Penetration Test Performance and Design*. J. H. Schmertmann, Report FHWA-TS-78-209, U.S. Department of Transportation, Washington.

Federal Highway Administration (FHWA) (2011). *Post-Earthquake Reconnaissance Report on Transportation Infrastructure: Impact of the February 27, 2010, Offshore Maule Earthquake in Chile*.

W.-H. P. Yen, G. Chen, I. Buckle, T. Allen, D. Alzamora, J. Ger, and J. G. Arias, Publication No. FHWA-HRT-11-030, U.S. Department of Transportation, McLean, VA.

Fleming, W. G. K., Weltman, A. J., Randolph, M. F., and Elson, W. K. (1985). *Piling Engineering*. Surrey University Press, London.

Franke, K. W. (2011). *A Performance-Based Model for the Computation of Kinematic Pile Response Due to Lateral Spread and its Application on Select Bridges Damaged During the M7.6 Earthquake in the Limon Province, Costa Rica*. Ph.D. Dissertation, Brigham Young University.

Geo-Engineering Extreme Events Reconnaissance (GEER) Association (2010). *Geo-engineering Reconnaissance of the 2010 Maule, Chile Earthquake*. J. Bray and D. Frost, eds., Report No. GEER-022.

Idriss, I. M. and Boulanger, R. W. (2007). "Residual shear strength of liquefied soils." *Proceedings of the 27th USSD Annual Meeting and Conference, Modernization and Optimization of Existing Dams and Reservoirs*.

Idriss, I. M. and Boulanger, R. W. (2008). *Soil Liquefaction During Earthquakes*. Earthquake Engineering Research Institute (EERI), MNO-12.

Janbu, N. (1973). "Slope stability computations." *Embankment Dam Engineering – Casagrande Volume*, R. C. Hirschfeld and S. J. Poulos, eds., John Wiley & Sons, New York. 47–86.

Kramer, S. L. (2008). *Evaluation of Liquefaction Hazards in Washington State*. Washington State Department of Transportation (WSDOT), WA-RD 668.1.

Kramer, S. L. and Mayfield, R. T. (2007). "Return period of soil liquefaction." *Journal of Geotechnical and Geoenvironmental Engineering, ASCE*, 133(7), 802–813.

Kulhawy, F. H. and Mayne, P. W. (1990). "Manual on estimating soil properties for foundation design." *Report no.*, Electric Power Research Inst., Palo Alto, CA (USA); Cornell Univ., Ithaca, NY (USA). Geotechnical Engineering Group. EPRI EL-6800, Project 1493-6 Final Report.

Ledezma, C. (2012). "Case study of three pile-supported bridges affected by liquefaction-induced lateral spreading after the M8.8 2010 Maule Chile earthquake." *Second International Conference on Performance-Based Design in Earthquake Geotechnical Engineering*, Taormina, Italy, May 28-30, Paper No. 6.13.

Ledezma, C. and Bray, J. D. (2010). "Probabilistic performance-based procedure to evaluate pile foundations at sites with liquefaction-induced lateral displacement." *Journal of Geotechnical and Geoenvironmental Engineering, ASCE*, 136(3), 464–476.

LPILE (2010). *A Program for the Analysis & Design of Piles and Drilled Shafts Under Lateral Loads*. `http://www.ensoftinc.com`. Ensoft, Inc. Engineering Software, Austin, Texas.

Martin, G. R., March, M. L., Anderson, D. G., Mayes, R. L., and Power, M. S. (2002). "Recommended design approach for liquefaction induced lateral spreads." *Proc., 3rd Natl. Seismic Conf. and Workshop on Bridges and Highways*, MCEER-02-SP04, Buffalo, NY.

Matlock, H. (1970). "Correlations for design of laterally loaded piles in soft clay." *Proceedings of the 2nd Offshore Technology Conference*, Houston, TX. (OTC 1204), 577–594.

McGann, C. R., Arduino, P., and Mackenzie-Helnwein, P. (2012). "Development of simplified analysis procedure for piles in laterally spreading layered soils." *PEER Report No. 2012/05*, Pacific Earthquake Engineering Research Center, University of California, Berkeley.

Meyerhof, G. G. (1956). "Penetration tests and bearing capacity of cohesionless soils." *Journal of the Soil Mechanics and Foundations Division, ASCE*, 82(SM1), 1–19.

Mokwa, R. L. and Duncan, J. M. (2001). "Laterally loaded pile groups and *p-y* multipliers." *Foundations and Ground Improvement: Proceedings of a specialty conference: June 9-13, Blacksburg, VA*, T. L. Brandon, ed., Geotechnical Special Publication No. 113. ASCE, 728–742.

Mokwa, R. L. and Duncan, J. M. (2003). "Rotational restraint of pile caps during lateral loading." *Journal of Geotechnical and Geoenvironmental Engineering, ASCE*, 129(9), 829–837.

National Cooperative Highway Research Program (NCHRP) (2002). *Comprehensive Specification for the Seismic Design of Bridges*. NCHRP Report 472, National Academy Press, Washington, D.C.

Olson, S. M. and Stark, T. D. (2002). "Liquefied strength ratio from liquefaction flow failure case histories." *Canadian Geotechnical Journal*, 39, 629–647.

Peck, R. B., Hanson, W. E., and Thornburn, T. H. (1974). *Foundation Engineering*. John Wiley & Sons, New York. 2nd Edition.

Petrus Consultores Geotecnicos (2006). *Informe Complementario de Mecánica de Suelos, Puente Mataquito (Ruta Costera), Camino Quivolgo-Iloca (Cruce J-60).* Informe No. 2619-ING-SGC-150/2006 (Rev 1).

Reese, L. C., Cox, W. R., and Koop, F. D. (1974). "Analysis of laterally loaded piles in sand." *Proceedings of the 6th Offshore Technology Conference*, Vol. 2, Houston, TX. 473–483.

Reese, L. C. and Van Impe, W. F. (2010). *Single piles and pile groups under lateral loading.* CRC Press.

Reese, L. C. and Welch, R. C. (1975). "Lateral loading of deep foundations in stiff clay." *Journal of the Geotechnical Engineering Division, ASCE*, 101(GT7), 633–649.

Rocscience (2010). *Slide 6.0 Slope Stability and Groundwater Software.* `http://www.rocscience.com`. Rocscience, Inc., Toronto, Ontario.

Seed, R. B. and Harder, L. F. (1990). "Spt-based analysis of cyclic pore pressure generation and undrained residual strength." *Proceedings of the H. Bolton Seed Memorial Symposium, Vol. 2*, Vancouver, BC, Canada. BiTech Pub, Ltd., 351–376.

Wang, C.-H. (2003). *Prediction of the Residual Strength of Liquefied Soils.* Ph.D. Dissertation, University of Washington.

Wu, J. (2002). *Liquefaction Triggering and Post-Liquefaction Deformation of Monterey 0/30 Sand Under Uni-Directional Cyclic Simple Shear Loading*, Vol. 1. University of California, Berkeley.

Youd, T. L., Hansen, C. M., and Bartlett, S. F. (2002). "Revised multilinear regression equations for prediction of lateral spread displacement." *Journal of Geotechnical and Geoenvironmental Engineering, ASCE*, 128(12), 1007–1017.

Youd, T. L., Idriss, I. M., Andrus, R. D., Arango, I., Castro, G., Christian, J. T., Dobry, R., Finn, W. D., Harder, L., Haynes, M. E., Ishihara, K., Koester, J. P., Liao, S. S. C., Marcuson, W. F., Martin, G. R., Mitchell, J. K., Moriwaki, Y., Power, M. S., Robertson, P. K., Seed, R. B., and Stokoe, K. H. (2001). "Liquefaction resistance of soils: Summary report from the 1996 NCEER and 1998 NCEER/NSF workshops on evaluation of liquefaction resistance of soils." *Journal of Geotechnical and Geoenvironmental Engineering, ASCE*, 127(10), 817–833.

Zha, J. (2004). "Lateral spreading forces on bridge abutment walls/piles." *Geotechnical Engineering for Transportation Projects*, M. K. Yegian and E. Kavazanjian, eds., GSP 126, ASCE. 1711–1720.

Americans with Disabilities Act (ADA) Information:
This material can be made available in an alternate format by emailing the Office of Equal Opportunity at wsdotada@wsdot.wa.gov or by calling toll free, 855-362-4ADA(4232). Persons who are deaf or hard of hearing may make a request by calling the Washington State Relay at 711.

Title VI Statement to Public:
It is the Washington State Department of Transportation's (WSDOT) policy to assure that no person shall, on the grounds of race, color, national origin or sex, as provided by Title VI of the Civil Rights Act of 1964, be excluded from participation in, be denied the benefits of, or be otherwise discriminated against under any of its federally funded programs and activities. Any person who believes his/her Title VI protection has been violated, may file a complaint with WSDOT's Office of Equal Opportunity (OEO). For additional information regarding Title VI complaint procedures and/or information regarding our non-discrimination obligations, please contact OEO's Title VI Coordinator at (360) 705-7082.